JOC The Journal of Organic Chemistry

Article

pubs.acs.org/joc

Mono- and Bisquinoline-Annulated Porphyrins from Porphyrin β,β′-Dione Oximes

Joshua Akhigbe,[†] Michael Luciano,[†] Matthias Zeller,[‡] and Christian Brückner*,[†]

[†]Department of Chemistry, University of Connecticut, Storrs, Connecticut 06269-3060, United States

[‡]Department of Chemistry, Youngstown State University, One University Plaza, Youngstown, Ohio 44555-3663, United States

Supporting Information

ABSTRACT: An acid-induced reaction of *meso*-tetraphenyl-2-hydroxyimino-3-oxoporphyrin leads, with concomitant loss of water, to a formal electrophilic aromatic substitution of the ortho-position of the phenyl group adjacent to the oxime, forming a quinoline moiety. Owing in part to the presence of a π-extended chromophore, the resulting *meso*-triphenylmonoquinoline-annulated porphyrin (λ_{max} = 750 nm) possesses a much altered optical spectrum from that of the starting oxime (λ_{max} = 667 nm). An oxidative DDQ-induced ring-closure process is also possible, generating the corresponding *meso*-triphenylmonoquinoline-annulated porphyrin quinoline *N*-oxide, possessing a slightly shifted and sharpened UV−vis spectrum (λ_{max} = 737 nm). The connectivity of the chromophores was conclusively shown by NMR spectroscopy. Both ketone functionalities in *meso*-tetraphenyl-2,3-dioxoporphyrin can be converted, via the oxime and using the acid- or oxidant-induced reaction pathways, either in one step or in a stepwise fashion, to bisquinoline-annulated porphyrin (λ_{max} = 775 nm) and its *N*-oxide (λ_{max} = 779 nm), respectively. This process is complementary to a previously established pathway toward bisquinoline-annulated porphyrins. Their zinc(II), nickel(II), and palladium(II) complexes are also described. Several examples of the quinoline-annulated porphyrins were crystallographically characterized, proving their connectivity and showing their conformations that are extremely distorted from planarity. The work presents a full account on the synthesis, structure, and spectroscopic properties of these classes of NIR-absorbing dyes.

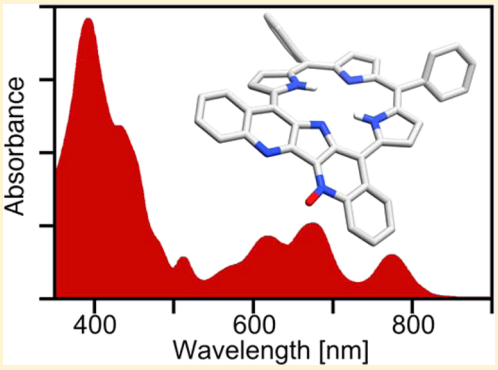

INTRODUCTION

Even though the high extinction coefficients, fluorescence, and singlet oxygen photosensitization quantum yields of regular porphyrins and chlorins are potentially attractive for their use in biomedical applications, e.g., as photochemotherapeutics,[1] photoantimicrobials,[2] photoantifungals,[3] or fluorescent markers,[1c,4] most regular porphyrins and chlorins do not absorb light within the ∼700−900 nm wavelength regime referred to as the "optical window" of tissue.[5] For instance, the maximum wavelength of absorbance (λ_{max}) for regular porphyrins, such as *meso*-tetraphenylporphyrin **1H$_2$**, rarely exceeds 650 nm. In comparison, the wavelength of maximum penetration of breast tissue is ∼725 nm; whole blood has an absorption minimum at ∼710 nm.[6] Regular porphyrins are thus unsuitable for biomedical *in vivo* applications. Nonemitting chromophores may also be attractive as photoacoustic imaging agents but,[8] again, only if they also absorb light within the optical window of tissue.[9] Light-harvesting applications also benefit from NIR-absorbing dyes, as a large portion of the irradiance energy of sunlight falls into this range. Panchromatic absorbers are also most desirable for light harvesting, as these chromophores collect the maximum amount of energy.[7]

A number of strategies have been employed to achieve this goal. For instance, the expansion of the conjugated π-system by increasing the number of conjugated pyrroles was greatly successful, as the many examples of NIR-absorbing expanded porphyrins demonstrate.[10] One other strategy is the establishment of π-systems that are annulated to the porphyrinic chromophore.[7d,11] Among the latter class of porphyrins may be *meso*-arylporphyrin derivatives that bear a covalent linkage between one or more β-positions and the flanking *meso*-phenyl/aryl groups.[12] In the absence of the linkage, a $H_{\beta\text{-pyrrole}}$−$H_{o\text{-phenyl}}$ steric interaction prevents the *meso*-aryl groups from adopting low-energy coplanar conformations. The linkage removes this interaction but needs to be short enough to force the phenyl group(s) into (idealized) coplanarity with the porphyrinic chromophore, thereby extending the π-conjugation pathway. This linkage may be a ketone functionality, itself in conjugation with the chromophore (**2H$_2$**).[13] The resulting bathochromic shift of λ_{max} of **2H$_2$** compared to **1H$_2$** is a respectable ∼76 nm. On the other hand, the fusion of one through four anthracenes to a porphyrin, as in **3H$_2$**, results in an enormous perturbation of their UV−vis spectra, with λ_{max} values red-shifted ∼300 nm upon fusion of a single anthracene; the corresponding nickel(II) complex with four anthracenes shifted the λ_{max} by more than 900 nm, to 1417 nm.[14] Few examples exist in which a chlorin chromophore incorporates an

Received: November 2, 2014
Published: December 3, 2014

annulated ring, as in bischromene-annulated chlorin $4H_2$, leading to a 24 nm-shifted λ_{max} compared to the parent chlorin.[15]

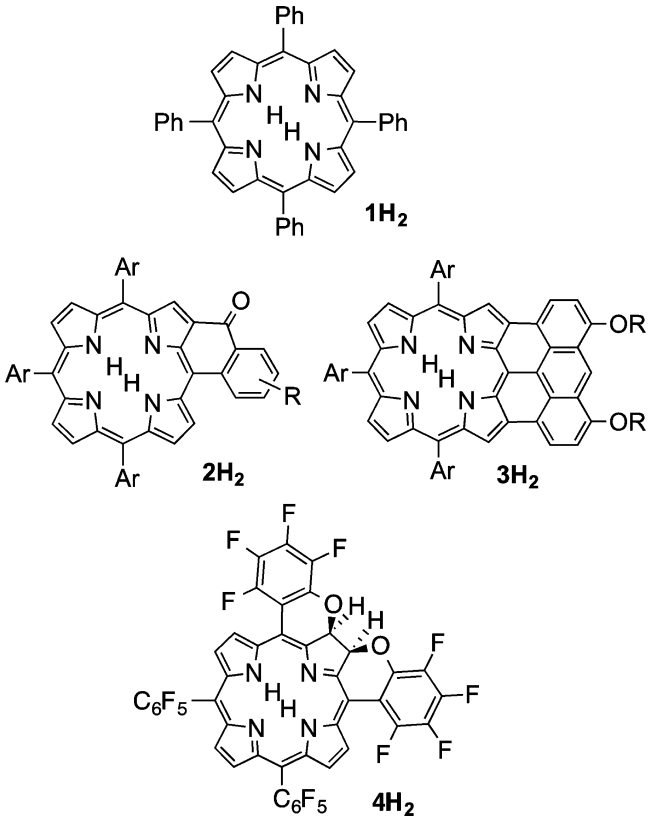

In 2011, Jeandon and Ruppert, building on the extensive work by Ruppert, Callot, and co-workers in the construction of peripherally conjugated chelates,[16] published the formation of bisquinoline-annulated porphyrin $7H_2$ from nickel porphyrin **1Ni** via a multistep sequence (Scheme 1).[17] The key *β*-to-*ortho*-linkage formation step involved a Cadogan reaction of nitroporphyrin **5Ni** to form the amine-linked porphyrin **6Ni**. Subsequent nitrogen protection, regioselective nitration, thermally induced oxidation and ring-closure, and acid-induced demetalation produced the bisquinoline-annulated system $7H_2$ in good yield.

Concurrently with Jeandon and Ruppert, we independently described in a preliminary report the conversion of free base porphyrin $1H_2$ to free base bisquinoline-annulated porphyrin $7H_2$.[18] The key steps were two consecutive acid-mediated electrophilic aromatic substitution reactions of oximes, such as $10H_2$, formed from the corresponding ketone $8H_2$. We prepared this well-known dione $8H_2$ along a dihydroxylation−diol oxidation sequence from porphyrin $1H_2$,[19] but this product can be made along a number of alternative routes.[20]

We follow up here on our preliminary report and present the full account on the formation and reactivity of the mono- and dioximes of $8H_2$ with respect to their conversion to a number of free base and metalated mono- and bisquinoline-annulated porphyrins, and their *N*-oxide derivatives. These chromophores are characterized by remarkably bathochromically shifted optical spectra when compared to regular porphyrins. We will also report the X-ray crystal structures of a number of derivatives, thus highlighting their nonplanar conformations we interpret as one reason for their red-shifted and broadened spectra. We recently demonstrated the efficacy of the quinoline-annulated porphyrins to act as photoacoustic imaging contrast agents in tissue phantom studies.[9]

RESULTS AND DISCUSSION

Synthesis of *meso*-Tetraphenylmonooxime $10H_2$ and -bisoxime $11H_2$. Analogous to the previously described conversion of the nickel(II) and palladium(II) complexes of porphyrin dione **8Ni** and **8Pd**,[21] free base 2,3-dioxoporphyrin $8H_2$ can also be converted to the corresponding monooxime $10H_2$ by reaction with ∼100-fold stoichiometric excess of hydroxylamine hydrochloride ($NH_2OH{\cdot}HCl$) in pyridine over 24 h at ambient temperature (Scheme 2). Its analytical and spectroscopic properties were similar to those of its

Scheme 1. Two Independent Paths toward Bisquinoline-Annulated Porphyrin $7H_2$ Developed by Ruppert (1Ni → 5Ni → $7H_2$) and Brückner ($1H_2$ → $10H_2$ → $7H_2$)

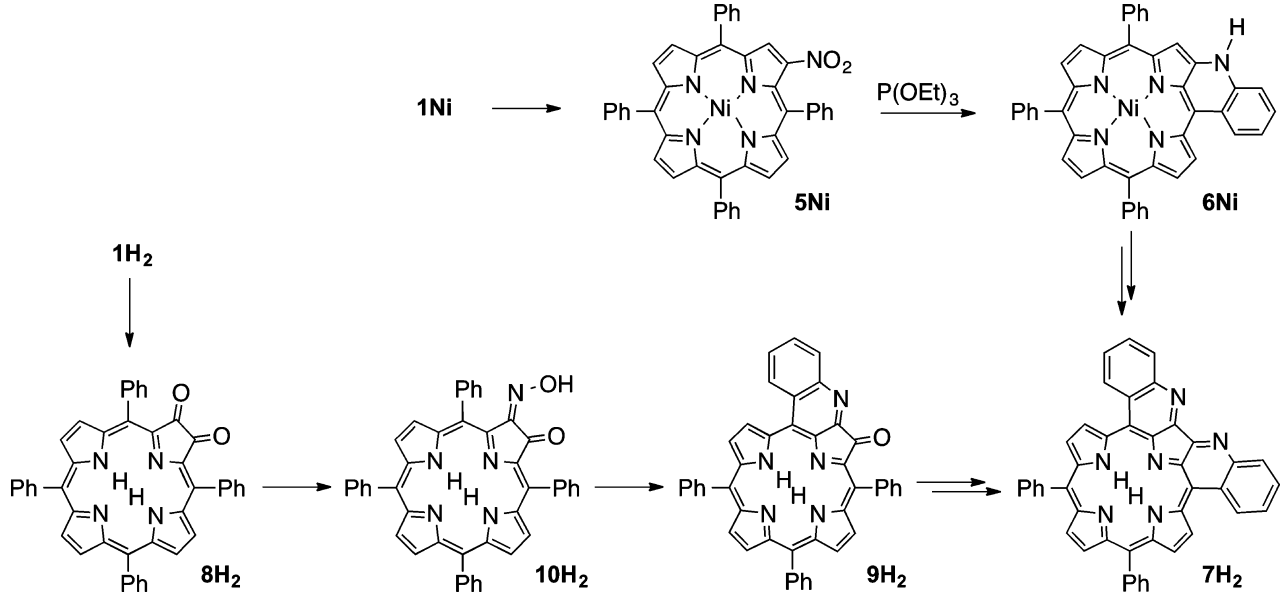

dx.doi.org/10.1021/jo502511j | J. Org. Chem. 2015, 80, 499−511

Scheme 2. Synthetic Pathways toward Monoquinoline-Annulated Porphyrins

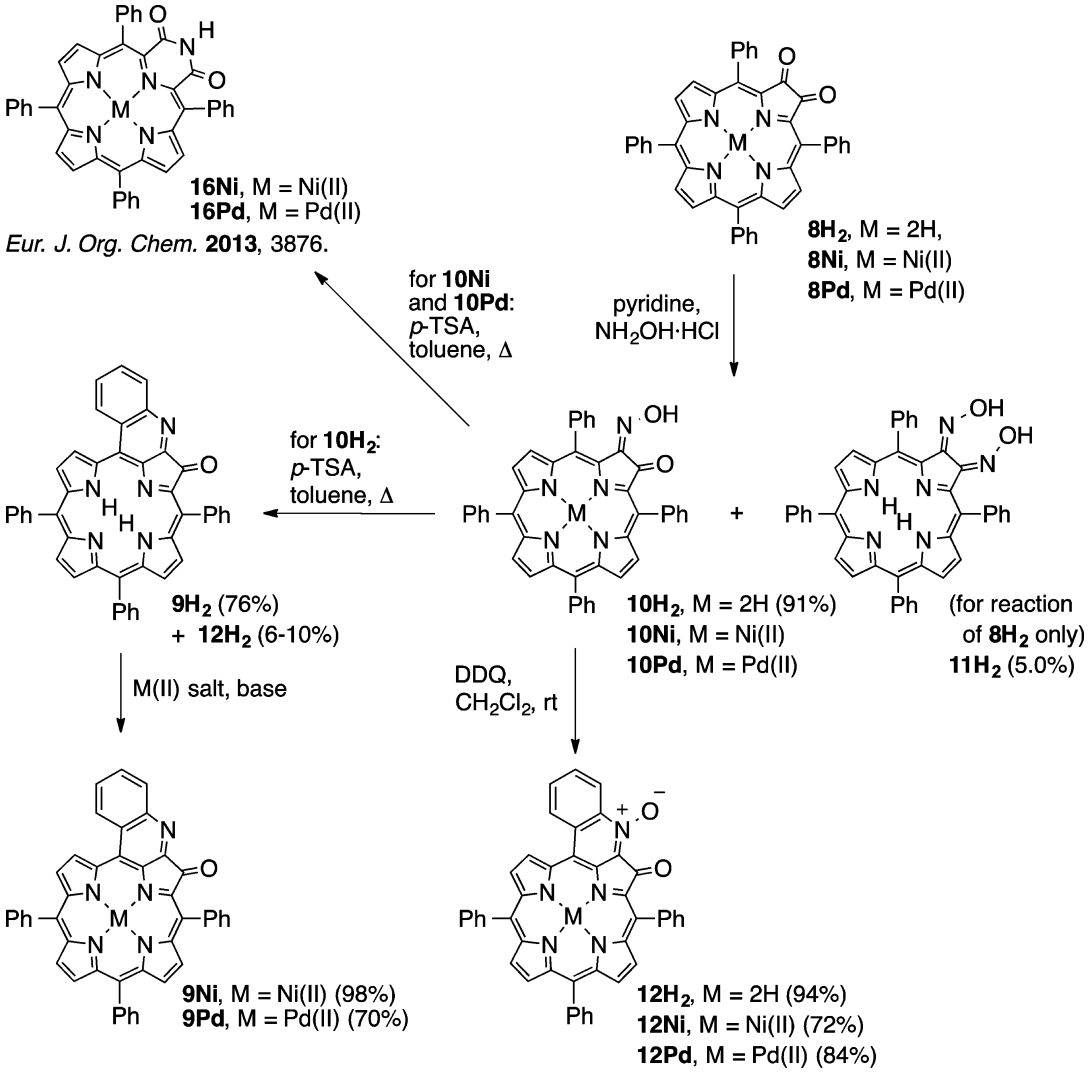

diamagnetic metal complexes: the ^{13}C NMR of **10H$_2$** indicated the presence of one carbonyl (188.2 ppm) and one imine carbon (151.8 ppm), functionalities that could also be confirmed by FT-IR spectroscopy ($\nu_{C=O}$ and $\nu_{C=N}$ at 1652.1 and 1548.6 cm^{-1}, respectively). A diagnostic ^{1}H NMR spectral feature for the monooximes is the signal at ~15.7 ppm (exchangeable with D_2O) that is assigned to the oxime hydrogen that is H-bonded to the neighboring carbonyl group (Figure 1). The structural characterization of **10Ni** by single crystal X-ray diffractometry is described below (Figure 4).

Next to the major product monooxime **10H$_2$**, a minor amount of the bisoxime **11H$_2$** could also be isolated, possessing all expected spectroscopic properties (see Supporting Information (SI) for details). The occurrence of the bisoxime was not observed in the reaction of the dione metallocomplexes **8Ni** and **8Pd**.[21]

The UV−vis spectra of free base dione **8H$_2$**, monooxime **10H$_2$**, and bisoxime **11H$_2$** are similar to each other in that all possess, compared to the regular porphyrin spectrum of *meso*-tetraphenylporphyrin **1H$_2$** (not shown), slightly broadened Soret bands and very broadened Q-bands (Figure 2). However, with increasing ketone-to-oxime transformations, the Q-band region becomes more defined, with increasingly sharper and distinctive peaks. The strong electronic effects of the *β*,*β*′-diketone functionality were discussed previously.[19,22] Evidently, this influence extends also to the oximes, albeit to a slightly lesser degree.

Formation of Free Base and Metalated Monoquinoline-Annulated Oxoporphyrins 9. Treatment of the olive-colored free base monooxime **10H$_2$** with a strong organic acid (*p*-TSA) under forcing conditions (toluene, reflux) generated a major light brown product, **9H$_2$**, with a mass indicating the loss of H_2O (HR-MS ESI+, 100% CH_3CN, suggests a composition of $C_{44}H_{28}N_5O$ for MH^+) (Scheme 2). As the oxime signal vanished from the ^{1}H NMR spectrum of the product, the oxygen lost likely stems from the oxime functionality (Figure 1). Further, the ^{1}H NMR spectrum of product **9H$_2$** lacks any axial symmetry: For instance, all six *β*-protons are non-equivalent. A diagnostic set of four peaks assigned to one phenyl group (confirmed by 2D NMRs; see SI) suggests establishment of a link between a phenyl group and a flanking *β*-position. Its proton signals are much shifted (between 9.0 and 7.6 ppm) because of the induced coplanarity of this phenyl group with the porphyrinic macrocycle. Indaphyrins, for example, have shown similarly diagnostic patterns for such *β*-to-*o*-phenyl linkages. The ^{13}C NMR and IR (neat) spectra of **9H$_2$** indicated the preservation of one *β*-imine and one *β*-

dx.doi.org/10.1021/jo502511j | J. Org. Chem. 2015, 80, 499−511

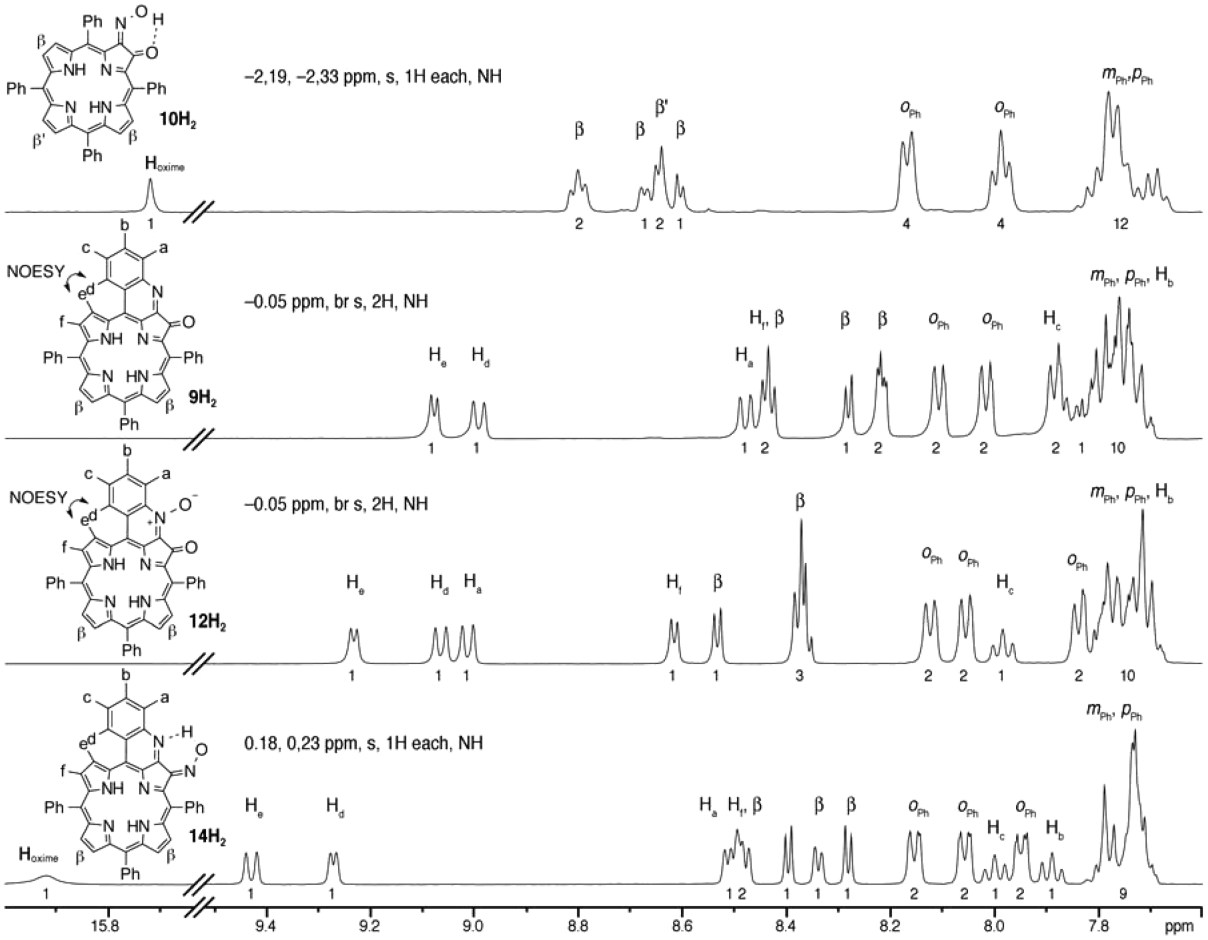

Figure 1. Comparison of the low-field region of the ^{1}H NMR spectra (400 MHz, $CDCl_3$, 25 °C) of the compounds indicated.

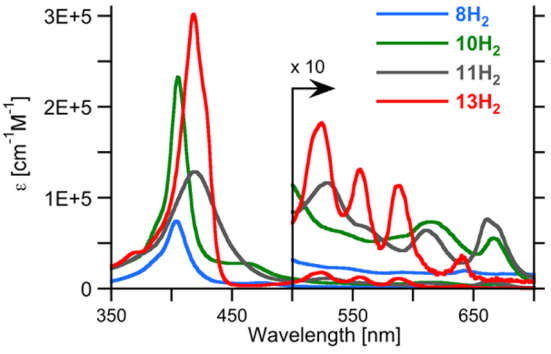

Figure 2. UV−vis spectra (CH_2Cl_2) of the compounds indicated.

ketone carbon (at 151 and 196 ppm, respectively). The summation of the spectroscopic data is suggestive of formation of the quinoline-annulated structure shown in Scheme 2. The UV−vis spectroscopic properties of this compound are, together with the optical spectra of all the other quinoline-annulated porphyrins, described below.

This outcome of the reaction highlights an interesting directing effect of the coordinated metal ion in light of the fact that the metal complexes of monooxime **10Ni** and **10Pd**, when reacted under identical acidic conditions, undergo a Beckmann rearrangement to form the corresponding *meso*-phenylpyrazinoporphyrin metal complexes **16M**.[21] This reactivity further implies that metal complexes of the quinoline-annulated porphyrin **9M** needed to be prepared by metal insertion into free base $\mathbf{9H_2}$. The corresponding metal insertion reactions using standard methodologies proceeded smoothly with good to excellent yields.[23] The composition (as determined by DART+ HR-MS) and spectroscopic data of **9Ni** and **9Pd** confirmed their expected quinoline-annulated porphyrin structures.

Alongside the major product $\mathbf{9H_2}$, we also isolated a minor product $\mathbf{12H_2}$ in yields ranging from 6% to 10%. Its mass, as determined by HR-MS, indicated the presence of an additional oxygen atom. Performance of the ring-closing reaction under inert conditions largely suppressed its formation. Consequently, the formation of this novel chromophore was traced to air oxidation. Product $\mathbf{12H_2}$ is also accessible as the major product from free base monooxime $\mathbf{10H_2}$ under oxidizing conditions.

Synthesis of Monoquinoline-Annulated Oxoporphyrin *N*-Oxides 12. Guided by the discovery of the oxidized quinoline-annulated product during the acid-catalyzed reaction, we discovered that this product can be prepared as the main product when free base monooxime $\mathbf{10H_2}$ is treated with DDQ at ambient temperatures (Scheme 2). Interestingly, the metal complexes of the oxime **10M** (M = Ni(II), Pd(II)) are also susceptible to this conversion, generating the metal analogues of the product, **12M** (M = Ni(II), Pd(II)). A careful $NaBH_4$ reduction of *N*-oxide $\mathbf{12H_2}$ regenerates $\mathbf{9H_2}$, though DDQ oxidation of $\mathbf{9H_2}$ does not lead to formation of $\mathbf{12H_2}$. This suggests that monoquinoline-annulated chromophore $\mathbf{9H_2}$ is not an intermediate in the formation of $\mathbf{12H_2}$. The oxidation of α,β-oximes of unsaturated substrates under a number of

dx.doi.org/10.1021/jo502511j | J. Org. Chem. 2015, 80, 499−511

Scheme 3. Synthetic Pathways toward Bisquinoline-Annulated Porphyrins

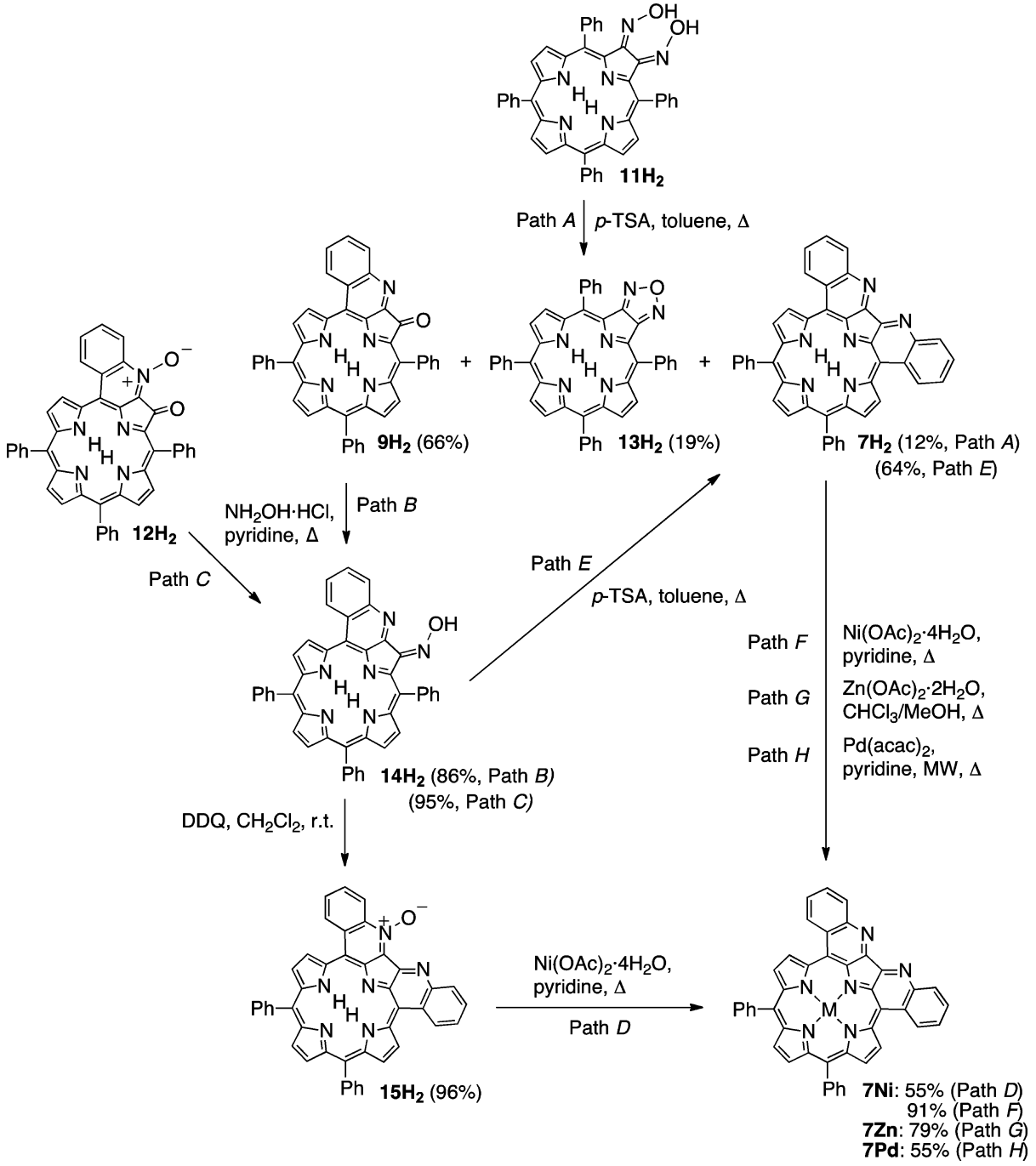

conditions frequently results in formation of iminoxy radical intermediates that undergo ring-cyclization reactions producing isoxazoles,[24] including isoxazoles annulated to a chlorin framework,[25] though the formation of quinoline *N*-oxides was also observed.[26] Presumably the formation of a six-membered quinoline ring in the cyclization of $\mathbf{10H_2}$ directs this reaction.

The presence of the oxygen atom in **12M** also has a strong influence on the UV−vis spectra of these chromophores when compared to the quinoline-annulated compounds **9M** (Figure 5; see discussion below). The NMR spectroscopic data for **12M** are significantly different from those of corresponding **9M** (Figure 1). Nonetheless, the same number of hydrogens and carbons are observed and the compound possesses the same overall symmetry by ^{1}H NMR spectroscopy (Figure 1). One hydrogen signal assigned to the CH group adjacent to the quinoline nitrogen is particularly strongly affected by the oxidation, suggestive of the presence of a quinoline *N*-oxide, as opposed to a porphyrin pyrrole *N*-oxide. The latter compounds are known, and their optical spectra are also severely distorted compared to those of the parent porphyrins.[27] A crystal structure analysis eventually provided unambiguous proof for the quinoline-annulated porphyrin quinoline *N*-oxide connectivity of product **12M** (Figure 4; all crystal structures are discussed below).

Synthesis of Monoquinoline-Annulated Oxoporphyrin Oxime $\mathbf{14H_2}$. Treatment of the β-keto functionality of free base monoquinoline $\mathbf{9H_2}$ with hydroxylamine hydrochloride under similar conditions as described above for the formation

dx.doi.org/10.1021/jo502511j | J. Org. Chem. 2015, 80, 499−511

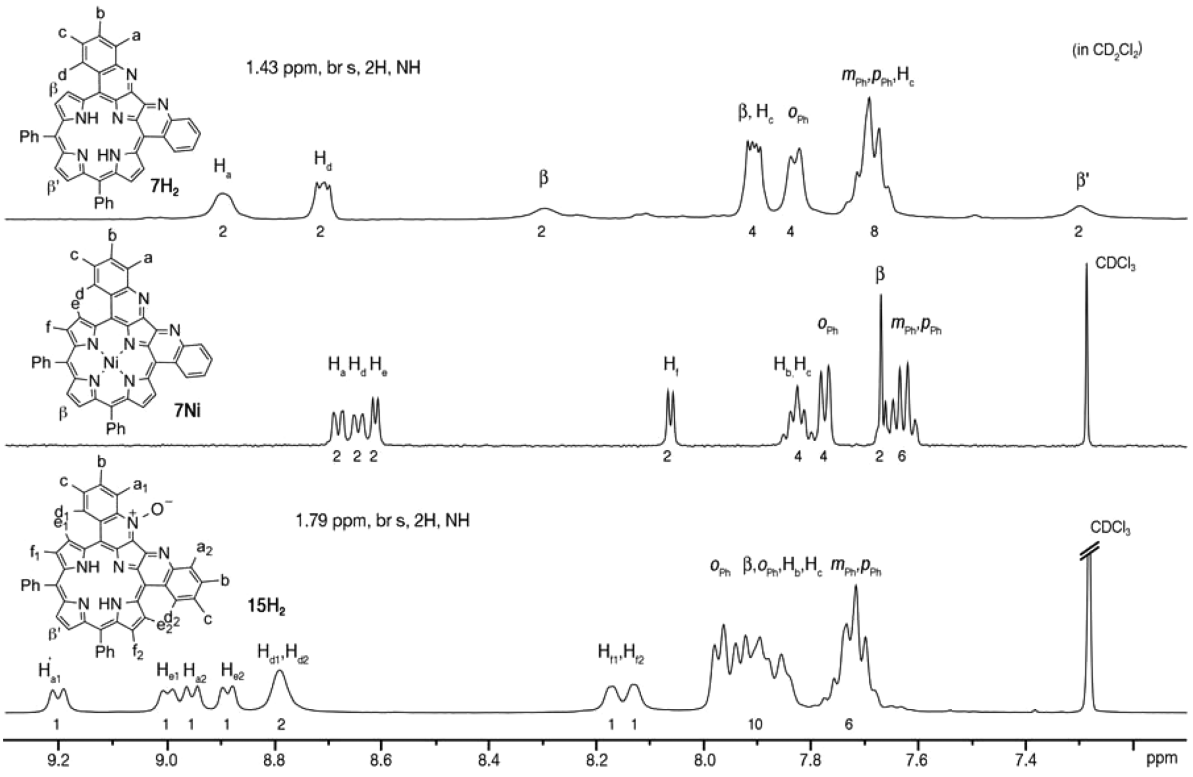

Figure 3. Comparison of the low-field region of the ^{1}H NMR spectra (400 MHz, in solvents indicated, 25 °C) of the bisquinoline-annulated porphyrins shown.

of the oximes **10H$_2$**/**10M** resulted in formation of oxime **14H$_2$** (Scheme 3). Similarly, reaction of *β*-keto *N*-oxide **12H$_2$** with hydroxylamine converted it to quinoline oxime **14H$_2$**. Note that the *N*-oxide moiety is lost in the process; such (reductive) losses are not unusual for heterocycle *N*-oxides.[28] Diagnostic peaks for the resulting oxime **14H$_2$** in the ^{1}H NMR spectrum are, analogous to oximes **10H$_2$**/**10M**, the signal for the strongly H-bonded oxime hydrogen (at ∼15.9 ppm) (Figure 1). All other spectroscopic and analytical data are as expected. The *β*-ketone-to-oxime conversion (**9H$_2$**/**12H$_2$** → **14H$_2$** conversion) perturbs the UV−visible spectrum of the products much more than the corresponding dione to oxime conversions (**8H$_2$** → **10H$_2$**/**11H$_2$** conversions, Figure 2; see also below).

Synthesis of Bisquinoline-Annulated Porphyrins 7H$_2$/7M and Bisquinoline-Annulated Porphyrin *N*-Oxide 15H$_2$. The oxime functionality shows analogous reactivity in both **10H$_2$** and the quinoline-annulated porphyrin **14H$_2$** (Scheme 3). Reaction of oxime **14H$_2$** with *p*-TSA under reflux conditions resulted in formation of a product in good yield that we were, based on its spectroscopic properties, able to identify as bisquinoline-annulated porphyrin **7H$_2$**; it possessed all the spectroscopic properties as reported by Jeandon and Ruppert,[17] including the broadened NMR spectra at rt attributed to extensive stacking and the limited solubility of this compound (Figure 3). Other annulated porphyrins have been observed to form tightly associated stacks in the crystal lattice.[14c] The synthetic routes presented here are thus alternative and fully independent routes toward a *π*-extended porphyrin chromophore with much altered optical properties (discussed below). The two pathways toward **7H$_2$** are complementary to each other. Both possess distinct advantages and disadvantages. The Jeandon and Ruppert synthesis is somewhat shorter (7 steps) versus our pathway (∼9 steps, depending in the chosen path toward the dione **8H$_2$**), and the overall yield of both syntheses are also similar (∼20%). One advantage of our route is its flexibility with respect to accessing other quinoline-annulated derivatives (such as the monoquinoline-annulated porphyrins and *N*-oxides).

The metal ions nickel(II), zinc(II), and palladium(II) could be inserted into free base **7H$_2$**, forming the corresponding metal complexes in good to satisfying yields. Metal insertion led to the formation of compounds that possess much sharpened ^{1}H NMR spectra (see Figure 3 for the spectrum of **7Ni**), presumably because of a lesser degree of stacking.

Reaction of oxime **14H$_2$** with DDQ led to a compound of the molecular mass of bisquinoline-annulated porphyrin **7H$_2$** plus an oxygen atom (as per ESI+ HR-MS). Its ^{1}H NMR spectrum also shows the loss of axial symmetry (Figure 3). This suggests the formation of bisquinoline *N*-oxide **15H$_2$**, an interpretation that could also be confirmed by single crystal X-ray diffractometry (discussed below). Nickel(II) insertion into the *N*-oxide led to loss of the *N*-oxide functionality and formation of **7Ni**.

A Shorter Route to Bisquinoline-Annulated Porphyrin 7H$_2$. The successful stepwise formation of bisquinoline-annulated porphyrin **7H$_2$** via the route dione **8H$_2$** → oxime **10H$_2$** → quinoline-annulated oxoporphyrin **9H$_2$** → quinoline-annulated oxoporphyrin oxime **14H$_2$** → **7H$_2$** prompts the question whether the direct conversion of bisoxime **11H$_2$** → **7H$_2$** can be accomplished (even though the formation of bisoxime **11H$_2$** is inefficient and could not be optimized in our hands). The answer is yes but at a loss of overall efficiency. Reaction of **11H$_2$** under the conditions leading to quinoline annulation generated the desired product **7H$_2$**, but in only 12% yield. The major product is quinoline-annulated oxoporphyrin **9H$_2$**. Evidently, hydrolysis of one of the oximes is faster than

dx.doi.org/10.1021/jo502511j | *J. Org. Chem.* 2015, 80, 499−511

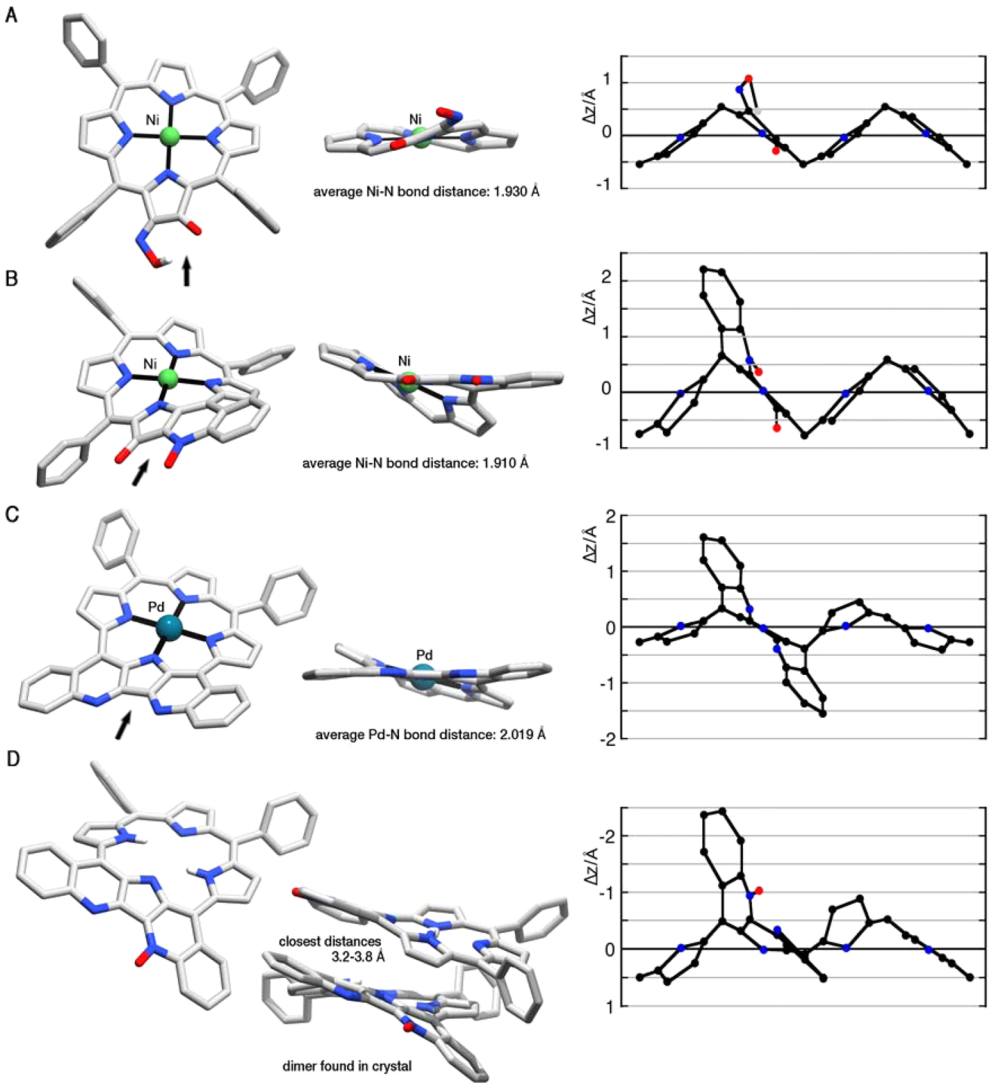

Figure 4. Stick representation of the X-ray single crystal structures: (A) **10Ni**; (B) **12Ni**; (C) **7Pd**; (D) **15H$_2$**. Top or oblique views (left column), side views (middle column), and deviation of the skeletal heavy atoms from the N_4 mean plane defined by the four pyrrolic nitrogens, as seen in the crystal structures (right column). All disorder and hydrogens bonded to carbon removed for clarity; phenyl groups removed for clarity in A, B, and C. Arrows indicate perspective for side views.

ring-closure. In fact, we observed fast hydrolysis of **11H$_2$** to form **10H$_2$**, even under the conditions of silica gel chromatography. The intramolecular condensation of the two oxime moieties with each other is also a more efficient process, generating oxadiazole (furazan)-annulated porphyrin **13H$_2$**. This novel product, related to Smith's pyrroloporphyrins,[29] shows very porphyrin-like optical properties (Figure 2) and was not further investigated (for details of **13H$_2$**, see also SI). In general, the condensation of α,β-bisoximes resulting in the formation of oxadiazoles is a well-known reaction.[30] Thus, even though the stepwise route toward product **11H$_2$** is significantly longer, its overall yield (~35% from diketone **11H$_2$**) is much better than the short route via bisoxime **11H$_2$** (<0.5% from diketone **11H$_2$**).

Reduction of Monoquinoline-Annulated Porphyrin 9H$_2$. Treatment of **9H$_2$** with $NaBH_4$ in CH_2Cl_2/10% MeOH at ambient temperatures yielded two polar products with a composition (as per ESI^+-MS) corresponding to $[M + 5H]^+$ and another, even more polar product, corresponding to $[M + 3H]^+$, suggestive of a reduction of either only the imine double bond (forming one isomer) or both the imine and the ketone double bonds (forming two diastereomers), respectively. The single double bond reduction product can also be made as the sole product using $NaBH_3CN$ at ice temperatures. Remarkably, all isolated products possessed much more blue-shifted, chlorin-like optical spectra with broadened Soret bands, highlighting the importance of the presence of the ketone and imine functionality for the electronic structure of the chromophore. Much to our disappointment, however, all three products proved to be intractable, as they all rapidly decomposed upon isolation at preparatively useful scales.

Structural Characterization of the Quinoline-Annulated Porphyrins. The considerably ruffled conformation of the monooxime **10Ni** is comparable to that observed in nickel(II) porphyrins and nickel dione **8Ni**[19] and like in these cases can be attributed to the small ionic radius of the low-spin nickel(II) (Figure 4).[31] The H-bond of the oxime moiety to the adjacent ketone functionality, seen in solution state (cf. to Figure 1), is also expressed in the solid state.

The crystal structure of the nickel(II) complex of quinoline-annulated porphyrin *N*-oxide **12Ni** provided the ultimate proof of the quinoline-annulated porphyrin connectivity, including

dx.doi.org/10.1021/jo502511j | J. Org. Chem. 2015, 80, 499−511

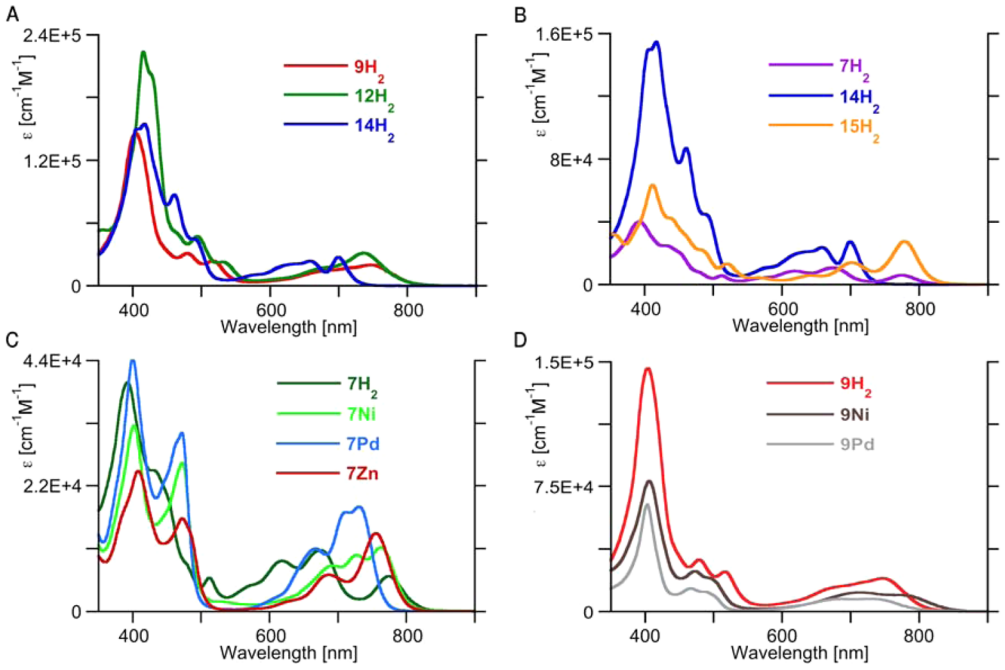

Figure 5. UV−vis spectra of the compounds indicated in CH_2Cl_2, except compound **7Zn** was, for solubility reasons, recorded in DMSO.

the presence of a quinoline *N*-oxide, as opposed to a central porphyrin pyrrole-*N*-oxide functionality. The ring-closure reaction of the oxime with the neighboring phenyl group generated a pyrrolo[3,2-*b*]quinolin-4-one moiety that is, presumably because of a steric interaction of this moiety with the *β*-hydrogen next to it, slightly bent. The prime conformation of the porphyrinic macrocycle is still ruffled, but it is strongly modulated by the presence of the quinoline-phenyl-to-*β*-H interaction. The *N*-oxide and ketone oxygens are eclipsed and form a potential metal binding pocket. Structurally related systems have been used for the formation of external metal complexes.[16c,d,f,32]

The Ni−N bond distances in primarily ruffled porphyrins can be used to gauge the degree of distortion. In **12Ni**, the Ni−N bond distances average 1.910 Å (ranging from 1.901 to 1.925 Å) and thus fall into the regime of a moderately nonplanar porphyrin. The Ni−N bond lengths in ruffled porphyrins shorten with the degree of ruffling. In comparison, the Ni−N bond lengths in lesser ruffled **10Ni** are 1.930 Å, and in only slightly ruffled **1Ni** 1.931 Å,[33] whereas they are 1.892 Å in an extremely ruffled nickel(II) secochlorin bisaldehyde.[31c]

The porphyrinoid macrocycle in free base bisquinoline-annulated *N*-oxide $\mathbf{15H_2}$ is particularly nonplanar, while the pentacyclic annulated heterocycle is slightly and asymmetrically bowed. The presence of palladium in the bisquinoline-annulated porphyrin **7Pd** planarizes the system somewhat when compared to the related free base $\mathbf{15H_2}$, but the porphyrinic chromophore is still considerably ruffled with significant saddling and waving modes. Despite these deformations, the metal is coordinated in a distorted square planar fashion, with regular average N−Pd bond distances of 2.019 Å (individual bonds range from 1.983 to 2.041 Å).[33]

Optical Properties of Quinoline-Annulated Porphyrins. Upon cyclization of monooxime $\mathbf{10H_2}$, the spectrum of quinoline-annulated porphyrin $\mathbf{9H_2}$ is much altered (Figure 5A): Most obvious, the Q-band region is much bathochromically shifted (for $\mathbf{10H_2}$, λ_{max} = 661 nm; for $\mathbf{9H_2}$, λ_{max} = 750 nm). Key to this is believed to be the extension of the conjugated *π*-system and the nonplanar conformation of $\mathbf{9H_2}$ (we extend from the conformation of its *N*-oxide $\mathbf{12H_2}$). The latter is also supported by the reduced extinction coefficient for the broadened Soret band of $\mathbf{10H_2}$.[34] Comparing the spectra of quinoline-annulated porphyrin $\mathbf{9H_2}$ with that of its *N*-oxide $\mathbf{12H_2}$, the distinct and sharpening effect of the quinoline N-oxidation (λ_{max} = 737 nm) and a red-shift of the Soret region can be noticed, highlighting the strong electronic effect the quinoline moiety has on the porphyrinic chromophore. Conversion of the oxo-group in $\mathbf{9H_2}$ to an oxime in $\mathbf{14H_2}$ (λ_{max} = 700 nm) similarly has a general sharpening effect on the Q-bands as the conversion of diketone $\mathbf{8H_2}$ to oxime $\mathbf{10H_2}$ (cf. to Figure 2).

Cyclization of quinoline-annulated porphyrin monooxime $\mathbf{14H_2}$ leads to the red-shifted spectrum of bisquinoline porphyrin $\mathbf{7H_2}$ described previously ($\mathbf{7H_2}$: λ_{Soret} = 392, λ_{max} = 775 nm) (Figure 5B).[17,18] Again, we attribute this shift to the conformation of the chromophore and the presence of the pentacyclic heterocycle that is *π*-conjugated with the porphyrinoid ring. As was observed for the oxidation of monoquinoline $\mathbf{9H_2}$, N-oxidation of $\mathbf{7H_2}$, forming $\mathbf{15H_2}$, also leads to a red-shift of its Soret band (λ_{Soret} = 412, λ_{max} = 779 nm). The closed-shell metal complexes of bisquinoline-annulated porphyrin $\mathbf{7H_2}$, **7Zn**, **7Ni**, and **7Pd** show, as expected, all similarly patterned spectra with a reduced number of Q-bands and a split Soret band (Figure 5C).

In contrast to the UV−vis spectra of metal complexes of bisquinoline $\mathbf{7H_2}$, the UV−vis spectra of the nickel and palladium complexes of monoquinoline porphyrin $\mathbf{9H_2}$, **9Ni** and **9Pd**, are not much different from those of the free base spectrum: they possess a much broadened Q-band region, with no sign of a split Soret band (Figure 5D). In this respect they are more similar to the metal complexes of dione $\mathbf{8H_2}$.

CONCLUSIONS

We demonstrated the annulation of a quinoline moiety onto a *meso*-tetraphenylporphyrin macrocycle by intramolecular ring

dx.doi.org/10.1021/jo502511j | J. Org. Chem. 2015, 80, 499−511

closure of the oximes of the well-known porphyrin 2,3-diones. This strategy can be applied twice in a stepwise fashion or, less efficiently, in a double-ring closure reaction of an α,β-bisoxime. Depending on the reagents used, a condensation reaction to form the quinoline-annulated ring-system takes place, or this condensation is also coupled with an oxidation, Thus, mono- and bisquinoline-annulated porphyrins and their quinolone *N*-oxides became accessible. These classes of porphyrin derivatives possess dramatically bathochromically shifted and broadened UV−vis spectra compared to the spectrum of the fundamental starting material porphyrin **1H$_2$**. This is attributed to the direct conjugation of the quinoline moiety with the aromatic porphyrinic π-system, the strong influence of β-oxo groups, and the nonplanarity of the chromophore. This synthesis of the bisquinoline-annulated porphyrin is an alternative to the synthesis presented by Jeandon and Ruppert.[17] The solid-state conformations of all quinoline-annulated porphyrins display pronounced deviations from planarity because of increased pyrrole-β-to-*o*-aryl interactions with the ring-annulated systems, while the polycyclic quinoline-annulated part of the compounds itself remains idealized planar or slightly curved. The conformation is modulated by the central metal present. The broad and intense absorption of the chromophores in the NIR region suggests their use in biomedical applications. However, their very low fluorescence and singlet oxygen quantum yields, reported earlier,[9] prevent their use as PDT agents, but we were able to show that this class of porphyrinoids is suitable as contrast agents for photoacoustic imaging applications.[9] We are currently in the process of preparing a range of quinoline-annulated porphyrins that possess more favorable solubility properties for their use in aqueous biological environments.

EXPERIMENTAL SECTION

Materials and Instruments. Solvents and reagents were used as received. Aluminum-backed, silica gel 60, 250 μm thickness analytical plates, 20 × 20 cm, glass-backed, silica gel 60, 500, or 1000 μm thickness preparative TLC plates, and standard grade, 60 Å, 32−63 μm flash column silica gel were used. Diones **8H$_2$**, **8Ni**, and **8Pd** were prepared as described previously.[19,21]

X-ray Single Crystal Diffractometry. Single crystals of **10Ni**, **12Ni**, **15H$_2$**, and **7Pd** were coated in mineral oil, mounted on a micromesh mount, and placed on a goniometer head under a stream of nitrogen cooled to 100 K. The data were collected on diffractometers using monochromatic Mo Kα (**15H$_2$**, **12Ni**, and **10Ni**) or Cu Kα radiation (**7Pd**) with the omega scan technique. Data were collected, their unit cells determined, and the data integrated and corrected for absorption and other systematic errors using the Apex2 suite of programs. The frames were integrated with the Bruker SAINT software package using a narrow-frame algorithm. Data were corrected for absorption effects using the multiscan method (SADABS). Space groups were assigned and the structures were solved by direct methods using the SHELXTL suite of programs and were refined by full matrix least-squares against F^2 with all reflections using Shelxl-97 or Shelxl2013 until the final anisotropic full-matrix, least-squares refinement of F^2 converged. Details of the data collection and structural parameters for the structure elucidations of **10Ni**, **12Ni**, **15H$_2$**, and **7Pd**, including complete cif files, descriptions of disorder, and hydrogen atom treatment, are presented in the SI.

***meso*-Tetraphenyl-2-hydroxyimino-3-oxoporphyrin (10H$_2$) and *meso*-Tetraphenyl-2,3-dihydroxyiminoporphyrin (11H$_2$).** *meso*-Tetraphenyl-2,3-dioxochlorin **8H$_2$** (120 mg, 1.85 × 10^{-4} mmol) was dissolved in pyridine (25 mL) in a round-bottom flask equipped with a magnetic stir bar and N_2 gas inlet. Hydroxylamine hydrochloride (H_2NOH·HCl, 1.2 g, ∼100 equiv) was added, and the mixture was stirred for 24 h at rt. When the starting material was consumed (reaction control by TLC), the reaction mixture was evaporated to dryness by rotary evaporation, taken up in CH_2Cl_2, and filtered through a glass frit (M). The volume of the filtrate was reduced and the mixture separated by column chromatography (silica−CH_2Cl_2/petroleum ether 3:1), allowing the isolation of **10H$_2$** in 91% (111 mg) and **11H$_2$** in 5.0% (6 mg) yields. **10H$_2$**: R_f (silica−CH_2Cl_2) = 0.75; ^{1}H NMR (400 MHz, $CDCl_3$): δ 15.7 (s, 1H, exchangeable with D_2O), 8.79 (t, ^3J = 4.0 Hz, 2H), 8.67−8.59 (m, 4H), 8.17 (d, ^3J = 8.0 Hz, 4H), 7.99 (t, ^3J = 8.0 Hz, 4H), 7.81−7.66 (m, 12H), −2.19 (s, 1H, exchangeable with D_2O), −2.33 (s, 1H, exchangeable with D_2O) ppm; ^{13}C NMR (100 MHz, $CDCl_3$): δ 188.2, 151.8, 145.7, 141.5, 141.4, 141.0, 139.9 138.9, 138.0, 134.6, 134.5, 134.0, 133.6, 132.8, 129.0, 128.8, 128.4, 128.3, 128.0, 127.9, 127.6, 127.2, 127.1, 124.1, 122.2, 116.5, 114.1 ppm; UV−vis (CH_2Cl_2) λ_{max} (log ε) 405 (5.37), 460 (4.45), 614 (3.87), 667 (3.75) nm; IR (neat, diamond ATR): see Figure S3, SI; HR-MS (ESI$^+$, cone voltage =30 V, 100% CH_3CN) *m*/*z* calcd for $C_{44}H_{30}N_5O_2$ ([M·H]$^+$) 660.2400, found 660.2381. **11H$_2$**: R_f (silica−CH_2Cl_2/1% MeOH) = 0.11; ^{1}H NMR (400 MHz, $CDCl_3$): δ 10.8−10.6 (br s, 1H), 8.71 (d, ^3J = 4.0 Hz, 1H), 8.54 (s, 1H), 8.45 (d, ^3J = 4.0 Hz, 1H), 8.14−8.12 (m, 2H), 8.03−7.98 (m, 2H), 7.78−7.70 (m, 6H), −2.09 (s, 1H, exchangeable with D_2O) ppm; ^{13}C NMR (100 MHz, $CDCl_3$): δ 154.7, 141.6, 141.5, 140.4, 137.2, 134.9, 134.8, 134.4, 133.9, 133.5, 128.5, 128.4, 128.2, 128.1, 127.6, 127.0, 123.4, 113.2 ppm; UV−vis (CH_2Cl_2) λ_{max} (log ε) 420 (5.11), 530 (4.05), 559 (sh), 610 (3.74), 661 (3.83) nm; IR (neat, diamond ATR): see Figure S12, SI; HR-MS (ESI$^+$, cone voltage = 30 V, 100% CH_3CN) *m*/*z* calcd for $C_{44}H_{31}N_6O_2$ ([M·H]$^+$) 675.2508, found 675.2515.

[*meso*-Tetraphenyl-2-hydroxyimino-3-oxoporphyrinato]-nickel(II) (10Ni). Prepared as nearly black shining crystals in 92% yield (69 mg, 0.96 × 10^{-4} mol) from *meso*-tetraphenyl-2,3-dioxoporphyrinato]nickel(II) (**8Ni**) (73 mg, 1.04 × 10^{-4} mol) in pyridine (25 mL) and H_2NOH·HCl (344 mg, ∼50 equiv) as described for **10H$_2$**: R_f (silica−CH_2Cl_2) = 0.70; ^{1}H NMR (500 MHz, $CDCl_3$): δ 15.3 (s, 1H, exchangeable with D_2O), 8.48 (d, ^3J = 4.8 Hz, 1H), 8.45, 8.43 (two overlapping d, ^3J = 4.9 Hz, 2H), 8.36, 8.34 (two overlapping d, ^3J = 5.2 Hz, 2H), 8.32 (d, ^3J = 4.9 Hz, 1H), 7.88 (d, ^3J = 7.2 Hz, 4H), 7.65−7.61 (m, 13H), 7.59−7.53 (m, 3H) ppm; ^{13}C NMR (125 MHz, $CDCl_3$): δ 184.2, 151.0, 146.0, 143.8, 143.5, 141.7, 140.4 140.0, 139.4, 137.7, 134.0, 133.9, 133.0, 132.9, 132.7, 132.3, 131.4, 130.9, 130.5, 129.9, 129.3, 128.2, 128.1, 127.7, 127.6, 127.4, 127.2, 124.5, 122.5, 116.1, 111.5 ppm; UV−vis (CH_2Cl_2) λ_{max} (log ε) 410 (5.50), 473 (4.73), 505 (sh), ∼560−800 (very broad band) nm; IR (neat, diamond ATR): see Figure S6, SI; MS (DART$^+$, orifice voltage = 20 V, 100% CH_3CN) *m*/*z* calcd for $C_{44}H_{28}N_5O_2Ni$ ([M·H]$^+$) 716.1596, found 716.1606.

[*meso*-Tetraphenyl-2-hydroxyimino-3-oxoporphyrinato]-palladium(II) (10Pd). Prepared in 77% yield (3.64 × 10^{-4} mol scale) from **8Pd** according to procedure described for **10H$_2$**: R_f (silica−CH_2Cl_2) = 0.82; ^{1}H NMR (400 MHz, $CDCl_3$): δ 15.9 (s, 1H, exchangeable with D_2O), 8.61 (d, ^3J = 5.0 Hz, 1H), 8.57 (d, ^3J = 5.0 Hz, 1H), 8.55 (d, ^3J = 5.2 Hz, 1H), 8.53 (d, ^3J = 5.0 Hz, 1H), 8.38 (d, ^3J = 5.1 Hz, 1H), 8.35 (d, ^3J = 5.0 Hz, 1H), 8.04 (d, ^3J = 7.9 Hz, 4H), 7.85 (d, ^3J = 8.1 Hz, 4H), 7.77−7.61 (m, 12H) ppm; ^{13}C NMR (100 MHz, $CDCl_3$): δ 185.2, 151.7, 145.6, 143.2, 142.3, 140.9, 140.6 140.2, 139.5, 133.8, 133.6, 133.5, 133.4, 132.9, 132.1, 132.0, 131.8, 130.8, 130.7, 130.2, 129.9, 129.7, 129.0, 128.6, 128.5, 128.4, 128.24, 128.20 127.6, 127.4, 127.3, 127.25, 127.23, 125.1, 119.8, 115.4 ppm; UV−vis (CH_2Cl_2) λ_{max} (log ε) 400 (5.29), 468 (4.48), 498 (4.23), ∼540−740 (br peak) nm; IR (neat, diamond ATR): see Figure S9, SI; MS (DART$^+$, orifice voltage = 20 V, 100% CH_3CN) *m*/*z* calcd for $C_{44}H_{28}N_5O_2Pd$ ([M·H]$^+$) 764.1293, found 764.1272.

Quinoline-Annulated Oxoporphyrin 9H$_2$. Free base monooxime **10H$_2$** (20.1 mg, 3.05 × 10^{-5} mol) was dissolved in toluene (10.0 mL) in a round-bottom flask equipped with a magnetic stir bar. To the stirring solution was added *p*-TSA (12 mg, 6.31 × 10^{-5} mol), and the mixture was heated to reflux for 30 min. When the starting material was consumed (reaction control by UV−vis and TLC), Et_3N (3 drops) was added and the mixture was evaporated to dryness by rotary evaporation. The residue was taken up in CH_2Cl_2 and filtered

dx.doi.org/10.1021/jo502511j | J. Org. Chem. 2015, 80, 499−511

through a plug of silica gel. The filtrate was washed with water (2 × 10 mL), dried over anhydrous Na_2SO_4, and evaporated to dryness by rotary evaporation. The residue was subjected to column chromatography (CH_2Cl_2−1%MeOH) to yield **9H$_2$** in 76% yield (15 mg): R_f (silica−CH_2Cl_2) = 0.23; ^{1}H NMR (500 MHz, CD_2Cl_2): δ 9.04 (d, ^3J = 4.5 Hz, 1H), 8.96 (d, ^3J = 7.5 Hz, 1H), 8.45 (d, ^3J = 8.0 Hz, 1H), 8.39 (t, ^3J = 5.0 Hz, 2H), 8.25 (d, ^3J = 4.5 Hz, 1H), 8.18 (t, ^3J = 4.0 Hz, 2H), 8.08 (d, ^3J = 7.0 Hz, 2H), 7.99 (d, ^3J = 7.0 Hz, 2H), 7.85−7.69 (m, 13H), −0.67 (br s, 2H, exchangeable with D_2O) ppm; ^{13}C NMR (100 MHz, CD_2Cl_2): δ 195.6, 151.4, 145.4, 143.8, 141.3, 141.1, 139.4, 137.1, 136.1, 135.0, 134.6, 134.1, 133.3, 133.1, 133.0, 132.9, 130.5, 130.4, 130.3, 129.0, 128.7, 128.6, 128.3, 128.2, 128.0, 127.7, 125.6, 123.8, 112.9, 109.1 ppm; UV−vis (CH_2Cl_2) λ_{max} (log ε) 405 (5.17), 480 (4.51), 518 (4.39), 674 (4.16), 750 (4.30) nm; IR (neat, diamond ATR): see Figure S18, SI; HR-MS (ESI$^+$, cone voltage = 30 V, 100% CH_3CN) m/z calcd for $C_{44}H_{28}N_5O$ ([M·H]$^+$) 642.2294, found 642.2316.

[Quinoline-annulated oxoporphyrinato]nickel(II) (9Ni). Free base **9H$_2$** (14.8 mg, 2.30 × 10^{-5} mol) was dissolved in pyridine (5 mL) and added to a hot solution of $Ni(CH_3CO_2)_2{\cdot}4H_2O$ (34.4 mg, 1.38 × 10^{-4} mol, 6.0 equiv) in pyridine (10 mL) in a round-bottom flask equipped with a magnetic stir bar. The mixture was heated to reflux for 12 h. When the starting material was consumed (reaction control by UV−vis and TLC), the resulting mixture was allowed to cool, the solvent was reduced to dryness by rotary evaporation, and the residue was taken up in minimal CH_2Cl_2 and subjected to flash column chromatography (silica−100% CH_2Cl_2) to yield the main product **9Ni** in 98% yield (16 mg): R_f (silica−CH_2Cl_2) = 0.14; ^{1}H NMR (400 MHz, $CDCl_3$): δ 8.72 (d, ^3J = 4.7 Hz, 1H), 8.41 (t, ^3J = 7.5 Hz, 2H), 8.30 (d, ^3J = 4.7 Hz, 1H), 8.10 (d, ^3J = 5.0 Hz, 1H), 7.94 (d, ^3J = 4.8 Hz, 1H), 7.89 (two overlapping d, 4.7 Hz, 2H), 7.77 (m, 5H), 7.69−7.56 (m, 12H) ppm; ^{13}C NMR (100 MHz, $CDCl_3$): δ 191.3, 150.6, 149.7, 145.1, 144.0, 143.3, 142.9, 140.6, 139.0, 138.9, 138.6, 137.0, 135.2, 135.1, 134.1, 133.1, 132.8, 132.7, 132.6, 131.6, 131.1, 130.6, 130.1, 129.9, 129.7, 129.2, 128.7, 128.6, 128.1, 128.0, 127.9, 127.8, 127.6, 127.2, 126.6, 116.1, 108.9 ppm; UV−vis (CH_2Cl_2) λ_{max} (log ε) 407 (4.89), 474 (4.39), 499 (4.31), 713 (4.05), 777 (3.99) nm; IR (neat, diamond ATR): see Figure S21, SI; MS (DART$^+$, orifice voltage = 20 V, 100% CH_3CN) m/z calcd for $C_{44}H_{26}N_5ONi$ 698.1491 ([M·H]$^+$), found 698.1498.

[Quinoline-annulated oxoporphyrinato]palladium(II) (9Pd). Free base **9H$_2$** (15.2 mg, 2.37 × 10^{-5} mol) was dissolved in benzonitrile (5 mL) and added to a hot solution of benzonitrile (15 mL) and $PdCl_2$ (8.5 mg, 4.79 × 10^{-5} mol, 2.0 equiv) in a round-bottom flask equipped with a magnetic stir bar and N_2 gas inlet, and the mixture was heated to reflux for 2 h. When the starting material was consumed (reaction control by UV−vis and TLC), the resulting mixture was allowed to cool, and the solvent was removed by rotary evaporation, taken up in the minimal quantity of CH_2Cl_2, and purified by flash column chromatography (silica gel−CH_2Cl_2/1% MeOH). The main green band was isolated to provide **9Pd** in 70% yield (13 mg): R_f (silica−CH_2Cl_2) = 0.25; ^{1}H NMR (400 MHz, $CDCl_3$): δ 9.00 (d, ^3J = 4.9 Hz, 1H), 8.78 (d, ^3J = 8.0 Hz, 1H), 8.49 (two overlapping d, ^3J = 7.0 Hz, ^4J = 1.1 Hz, 1H), 8.43 (d, ^3J = 5.0 Hz, 1H), 8.18 (d, ^3J = 5.1 Hz, 1H), 8.15 (s, 2H), 7.99−7.97 (m 3H), 7.92−7.90 (two overlapping d, ^3J = 6.3 Hz, ^4J = 1.8 Hz, 2H), 7.80−7.63 (m, 13H) ppm; ^{13}C NMR (100 MHz, $CDCl_3$): δ 191.1, 150.4, 148.4, 145.2, 142.4, 141.3, 140.3, 140.1, 139.8, 138.2, 134.0, 133.9, 133.5, 133.4, 133.3, 133.1, 133.0, 132.2, 131.9, 131.5, 130.0, 129.7, 129.6, 129.4, 129.2, 128.7, 128.6, 128.1, 127.9, 127.7, 127.4, 127.2, 126.9, 117.5, 111.0 ppm; UV−vis (CH_2Cl_2) λ_{max} (log ε) 406 (4.79), 471 (4.07), 738 (3.11) nm; IR (neat, diamond ATR): see Figure S24, SI; MS (DART$^+$, orifice voltage = 20 V, 100% CH_3CN) m/z calcd for $C_{44}H_{26}N_5OPd$ 746.1193 ([M·H]$^+$), found 746.1204.

Monoquinoline-Annulated Porphyrin Quinoline *N*-Oxide 12H$_2$. Monooxime **10H$_2$** (12 mg, 1.74 × 10^{-5} mol) was dissolved in CH_2Cl_2 (10 mL) in a round-bottom flask equipped with a magnetic stir bar. DDQ (8 mg, 3.5 × 10^{-5} mol, 2 equiv) was added, and the mixture was stirred for 30 min. When the starting material was consumed (reaction control by TLC), the reaction mixture was filtered through a short plug of silica gel. The filtrate was washed with water (2 × 10 mL), dried over anhydrous Na_2SO_4, and evaporated to dryness by rotary evaporation. The crude product was purified on a preparative TLC plate (silica−CH_2Cl_2/2% MeOH) to provide **12H$_2$** in 94% yield (11 mg): R_f (silica−CH_2Cl_2/5% MeOH) = 0.72; ^{1}H NMR (500 MHz, $CDCl_3$): δ 9.21 (d, ^3J = 5.0 Hz, 1H), 9.06 (d, ^3J = 8.0 Hz, 1H), 9.00 (d, ^3J = 7.5 Hz, 1H), 8.58 (d, ^3J = 5.0 Hz, 1H), 8.50 (d, ^3J = 5.0 Hz, 1H), 8.35−8.31 (m, 3H), 8.11 (d, ^3J = 8.0 Hz, 2H), 8.04 (d, ^3J = 8.0 Hz, 2H), 7.96 (t, ^3J = 7.5 Hz, 1H), 7.81 (d, ^3J = 8.0 Hz, 2H), 7.78−7.70 (m, 10H), −0.05 (br s, 2H, exchangeable with D_2O) ppm; ^{13}C NMR (125 MHz, $CDCl_3$): δ 184.6, 155.6, 153.7, 146.4, 144.9, 143.7, 141.2 141.0, 140.8, 138.7, 138.1, 136.3, 135.7, 134.3, 134.1, 133.7, 133.4, 132.4, 132.3, 131.1, 130.8, 129.5, 128.4, 128.2, 127.7, 127.5, 127.3, 127.0, 126.9, 125.3, 123.3, 121.9, 114.2, 101.5 ppm; UV−vis (CH_2Cl_2) λ_{max} (log ε) 416 (5.35), 427 (sh), 496 (4.67), 534 (4.67), 668 (4.21), 737 (4.49) nm; IR (neat, diamond ATR): see Figure S29, SI; MS (ESI$^+$, cone voltage = 30 V, 100% CH_3CN) m/z calcd for $C_{44}H_{28}N_5O_2$ ([M·H]$^+$), 658.2243 found 658.2213.

[Monoquinoline-annulated porphyrinato quinoline *N*-oxide]nickel(II) 12Ni. Prepared and purified using a preparative TLC plate (CH_2Cl_2/2% MeOH) in 72% yield from **10Ni** (2.20 × 10^{-5} mol scale) according to the general procedure for **12H$_2$**: R_f (silica−CH_2Cl_2/5% MeOH) = 0.84; ^{1}H NMR (500 MHz, $CDCl_3$): δ 8.89 (d, ^3J = 7.6 Hz, ^3J = 1.1 Hz, 1H), 8.80 (d, ^3J = 4.9 Hz, 1H), 8.46 (d, ^3J = 8.0 Hz, 1H), 8.42 (d, ^3J = 5.0 Hz, 1H), 8.19 (d, ^3J = 4.9 Hz, 1H), 8.09 (d, ^3J = 4.9 Hz, 1H), 8.04 (d, ^3J = 4.9 Hz, 1H), 8.00 (d, ^3J = 4.8 Hz, 1H), 7.87 (t, ^3J = 7.2 Hz 1H), 7.81−7.78 (m, 4H), 7.70 (t, ^3J = 7.0 Hz 1H), 7.66−7.56 (m, 11H) ppm; ^{13}C NMR (125 MHz, $CDCl_3$): δ 181.5, 148.4, 143.4, 142.9, 142.1, 140.9, 140.3, 138.9, 138.7, 136.9, 135.4, 134.1, 133.8, 133.7, 132.7, 132.6, 132.1, 131.3, 131.2, 130.7, 130.5, 130.0, 129.3, 128.6, 128.4, 128.3, 127.8, 127.7, 127.5, 127.4, 127.3, 127.1, 126.9, 121.7, 116.8, 100.7 ppm; UV−vis (CH_2Cl_2) λ_{max} (log ε) 420 (5.14), 493 (4.59), ∼580−860 (br peak) nm; MS (DART$^+$, orifice voltage = 20 V, 100% CH_3CN) m/z calcd for $C_{44}H_{26}N_5O_2Ni$ 714.1440 ([M·H]$^+$), found 714.1457.

[Monoquinoline-annulated porphyrinato quinoline *N*-oxide]palladium(II) 12Pd. Prepared and purified using a preparative TLC plate (CH_2Cl_2/2% MeOH) in 84% yield from **10Pd** (2.67 × 10^{-5} mol scale) according to the general procedure for **12H$_2$**: R_f (silica−CH_2Cl_2/5% MeOH) = 0.70; ^{1}H NMR (400 MHz, $CDCl_3$): δ 9.00 (d, ^3J = 5.0 Hz, 1H), 8.88 (dd, ^3J = 7.4 Hz, ^4J = 1.0 Hz, 1H), 8.71 (d, ^3J = 8.2 Hz 1H), 8.53 (d, ^3J = 5.0 Hz, 1H), 8.28 (d, ^3J = 4.8 Hz, 2H), 8.23 (d, ^3J = 4.9 Hz, 1H), 8.10 (d, ^3J = 4.9 Hz, 1H), 8.10 (two overlapping d, ^3J = 6.3 Hz, ^4J = 1.7 Hz, 2H), 7.95 (two overlapping d, ^3J = 6.3 Hz, ^4J = 1.6 Hz, 2H), 7.81 (t, ^3J = 7.0 Hz, 1H), 7.75−7.63 (m, 12H) ppm; UV−vis (CH_2Cl_2) λ_{max} (log ε) 416 (5.12), 489 (4.44), 664 (sh), 718 (4.19) nm; IR (neat, diamond ATR): see Figure S33, SI; MS (DART$^+$, orifice voltage = 20 V, 100% CH_3CN) m/z calcd for $C_{44}H_{26}N_5O_2Pd$ 762.1121 ([M·H]$^+$), found 762.1137.

Monoquinoline-Annulated Oxoporphyrin Oxime 14. Either monoquinoline-annulated oxoporphyrin **9H$_2$** (51.8 mg, 8.1 × 10^{-5} mmol) (path B, Scheme 3) or the corresponding *N*-oxide **12H$_2$** (60 mg, 9.1 × 10^{-5} mmol) (path C, Scheme 3) was dissolved in pyridine (20 mL) in a round-bottom flask equipped with a magnetic stir bar and N_2 gas inlet. Solid $H_2NOH{\cdot}HCl$ (80 mg) was added, and the mixture was heated to reflux for 2 h. When the starting material was consumed (reaction control by TLC), the reaction mixture was allowed to cool, the solvent was removed by rotary evaporation and dissolved in some CH_2Cl_2 (∼10 mL), and the mixture was filtered through a glass frit (M). The volume of the filtrate was reduced and loaded onto a flash chromatography column (silica−CH_2Cl_2/petroleum ether 3:1). Product **14H$_2$** was isolated in 86% (46 mg, path B) or 90% (54 mg, path C) yield. Alternatively, the reaction can be performed at ambient temperature for 36 h with comparable yields R_f (silica−CH_2Cl_2) = 0.35; ^{1}H NMR (400 MHz, $CDCl_3$): δ 15.9 (s, 1H, exchangeable with D_2O), 9.42 (d, ^3J = 8.0 Hz, 1H), 9.27 (d, ^3J = 4.0 Hz, 1H), 8.50−8.46 (m, 3H), 8.38 (d, ^3J = 4.0 Hz, 1H), 8.32 (d, ^3J = 4.0 Hz, 1H), 8.26, (d, ^3J = 4.0 Hz, 1H), 8.14−8.12 (m, 2H), 8.05−8.02 (m, 2H), 7.97 (t, ^3J = 8.0 Hz, 1H), 7.94−7.91 (m, 2H), 7.86 (t, ^3J = 8.0 Hz, 1H) 7.77−7.67 (m, 10H), 0.23 (s, 1H, exchangeable with

dx.doi.org/10.1021/jo502511j | J. Org. Chem. 2015, 80, 499−511

D_2O), 0.18 (s, 1H, exchangeable with D_2O) ppm; the limited solubility of this compound prevented the recording of high-quality ^{13}C NMR spectra; UV−vis (CH_2Cl_2) λ_{max} (log ε) 406 (sh), 417 (5.19), 461 (sh), 489 (sh), 574 (sh), 635 (sh), 659 (4.37), 700 (4.43) nm; IR (neat, diamond ATR): see Figure S39, SI; MS (ESI$^+$, cone voltage = 30 V, 100% CH_3CN) m/z calcd for $C_{44}H_{29}N_6O$ ([M·H]$^+$) 657.2403, found 657.2414.

***meso*-Tetraphenyloxadiazoleporphyrin $13H_2$ and Bisquinoline-Annulated Porphyrin $7H_2$.** Path A (Scheme 3): Bisoxime $\mathbf{11H_2}$ (13.3 mg, 1.97×10^{-5} mol) was dissolved in toluene (10 mL) in a round-bottom flask equipped with a magnetic stir bar, *p*-TSA (7.5 mg, 4.0×10^{-5} mol, ∼2.0 equiv) was added, and the mixture was heated to reflux for 30 min. When the starting material was consumed (reaction control by TLC), Et_3N (2 drops) was added and the mixture was evaporated to dryness by rotary evaporation. The residue was taken up in CH_2Cl_2 and filtered through a plug of silica gel. The filtrate was washed with water (2 × 10 mL), dried over anhydrous Na_2SO_4, and evaporated to dryness by rotary evaporation. The residue was separated on a preparative TLC plate (silica−CH_2Cl_2/petroleum ether 1:1) to furnish brown $\mathbf{9H_2}$ in 66% (8.3 mg), purple $\mathbf{13H_2}$ in 19% (2.5 mg), and green $\mathbf{7H_2}$ in 12% (1.5 mg) yields. Path E (Scheme 3): Bisquinoline-annulated porphyrin $\mathbf{7H_2}$ was prepared in 64% isolated yield from monofused oxime **14** using the procedure described in path A. Only minimal hydrolysis of the oxime and no *meso*-tetraphenyloxadiazoleporphyrin $\mathbf{13H_2}$ was observed. $\mathbf{13H_2}$: R_f (silica−CH_2Cl_2) = 0.86; ^1H NMR (400 MHz, $CDCl_3$): δ 8.95 (d, ^3J = 4.0 Hz, 1H), 8.86 (d, ^3J = 4.0 Hz, 1H), 8.71 (s, 1H), 8.21 (d, ^3J = 8.0 Hz, 2H), 8.16 (d, ^3J = 8.0 Hz, 2H), 7.89−7.74 (m, 6H), −2.72 (s, 1H, exchangeable with D_2O) ppm; ^{13}C NMR (100 MHz, $CDCl_3$): δ 163.8, 155.4, 141.7, 140.8, 139.1, 138.0, 137.5, 134.7, 134.6, 133.4, 129.1, 129.0, 128.3, 128.0, 127.8, 127.1, 123.2, 117.3 ppm; UV−vis (CH_2Cl_2) λ_{max} (log ε) 418 (5.48), 524 (4.27), 586 (4.13), 588 (4.08), 641 (3.60) nm; IR (neat, diamond ATR): see Figure S37, SI; MS (ESI$^+$, cone voltage = 30 V, 100% CH_3CN) m/z calcd for $C_{44}H_{29}N_6O$ ([M·H]$^+$) 657.2403, found 657.2413. $\mathbf{7H_2}$ (the spectroscopic data corresponds well to the data reported by Jeandon and Ruppert and is included here for comparison):[17] R_f (silica−CH_2Cl_2/1% MeOH) 0.30; ^1H NMR (400 MHz, CD_2Cl_2, 25 °C): δ 8.89 (br s, 1H), 8.71−8.69 (m, 1H), 8.28 (br s, 1H), 7.90 (d, two overlapping doublets, ^3J = 4.0 Hz, 2H), 7.83 (d, ^3J = 8.0 Hz, 2H), 7.71−7.67 (m, 4H), 7.40 (d, ^3J = 4.0 Hz, 2H), 7.30 (br s, 1H), 1.43 (br s, 1H) ppm; see Jeandon and Ruppert for high-temperature data; limited solubility at rt does not allow the recording of high-quality ^{13}C NMR spectra; UV−vis (CH_2Cl_2) λ_{max} (log ε) 392 (4.60), 432 (sh), 513 (3.77), 571 (sh), 619 (3.95), 675 (4.03), 775 (3.79) nm; IR (neat, diamond ATR): see Figure S41, SI; MS (ESI$^+$, cone voltage = 30 V, 100% CH_3CN) m/z calcd for $C_{44}H_{27}N_6$ ([M·H]$^+$) 639.2292, found 639.2294.

[Bisquinoline-annulated porphyrinato]nickel(II) (7Ni). Free base $\mathbf{7H_2}$ (11.5 mg, 1.8×10^{-5} mol) or free base $\mathbf{15H_2}$ (11.4 mg, 1.7×10^{-5} mol) (path D, Scheme 3) was dissolved in pyridine (5 mL) and added to a hot solution of pyridine (10 mL) and $Ni(CH_3CO_2)_2{\cdot}4H_2O$ (27 mg, 1.08×10^{-4} mol, 6.0 equiv) in a round-bottom flask equipped with a magnetic stir bar. The mixture was heated to reflux for 30 min. When the starting material was consumed (reaction control by UV−vis and TLC), the resulting mixture was allowed to cool, and the solvent was removed by rotary evaporation and taken up in minimal CH_2Cl_2. The crude product was separated on a preparative TLC plate (CH_2Cl_2/5% MeOH) to furnish green **7Ni** in 91% (11.7 mg, path F) or 55% (7.1 mg, path D) yields, respectively. The spectroscopic data corresponds well to the data reported by Jeandon and Ruppert and is included here for comparison:[17] R_f (silica−CH_2Cl_2/2% MeOH) = 0.19; ^1H NMR (500 MHz, $CDCl_3$): δ 8.65 (d, 7.5 Hz, 1H), 8.62 (d, 7.5 Hz, 1H), 8.58 (d, ^3J = 4.5 Hz, 1H), 8.03 (d, ^3J = 4.5 Hz, 1H), 7.82−7.77 (m, 2H), 7.50 (d, 2H), 7.64 (s, 1H) 7.62−7.58 (m, 3H) ppm; ^{13}C NMR (100 MHz, $CDCl_3$): δ 151.1, 147.5, 145.0, 143.9, 139.1, 138.8, 135.5, 132.7, 132.6, 131.9, 130.9, 129.9, 129.6, 128.7, 127.9, 127.7, 127.6, 126.5, 124.8, 109.6 ppm; UV−vis (CH_2Cl_2) λ_{max} (log ε) 402 (4.52), 473 (4.42), 691 (3.91), 727 (4.00), 765 (4.05) nm; IR (neat, diamond ATR): see Figure S44, SI; MS (ESI$^+$, cone voltage = 30 V, 100% CH_3CN) m/z calcd for $C_{44}H_{25}N_6Ni$ ([M·H]$^+$) 695.1489, found 695.1488.

[Bisquinoline-annulated porphyrinato]zinc(II) (7Zn). Bisquinoline porphyrin $\mathbf{7H_2}$ (11.5 mg, 1.8×10^{-5} mol) was dissolved in warm chloroform (10 mL) in a round-bottom flask equipped with a magnetic stir bar. A warm solution of $Zn(OAc)_2$ (3 equiv) in MeOH (1 mL) was added and the mixture heated to reflux for 1 h. When the starting material was consumed (reaction control by UV−vis and TLC), the mixture was diluted with MeOH (15 mL) and allowed to cool to ambient temperature, and the precipitated product was filtered off and dried to yield **7Zn** in 79% (10 mg) yield: R_f (silica−CH_2Cl_2/2% MeOH) = 0.54; ^1H NMR (400 MHz, DMSO-d_6): δ 9.15 (d, ^3J = 7.6 Hz, 1H), 8.74 (m, ^3J = 11.0 Hz, 2H). 8.01−7.89 (m, 5H), 7.73 (s, 3H), 7.54 (s, 1H) ppm; high quality ^{13}C NMR spectra could not be obtained because of the limited solubility of this complex; UV−vis (DMSO) λ_{max} (log ε) 329 (4.21), 409 (4.40), 473 (4.21), 687 (3.80), 756 (4.14) nm; MS (ESI$^+$, 100% CH_3CN, TOF) m/z cald for $C_{44}H_{25}N_6Zn$ ([M·H$^+$]) 701.1432, found 701.1448.

[Bisquinoline-annulated porphyrinato]palladium(II) (7Pd). Free base bisquinoline porphyrin $\mathbf{7H_2}$ (11.8 mg, 1.8×10^{-5} mol) was dissolved in pyridine (2.7 mL) in a thick-walled 2 cm OD glass tube equipped with a magnetic stir bar. $Pd(acac)_2$ (16.4 mg, 5.4×10^{-5} mol, 3 equiv) was added, and the vessel was sealed and placed in a microwave cavity. Using an initial microwave power of 300 W, the contents of the reaction vessel were heated to 180 °C where it was held for 15 min. Upon completion, the vessel was cooled to ambient temperature, the solvent was evaporated to dryness using rotary evaporation, and the residue was separated on a preparative TLC plate (CH_2Cl_2/2% MeOH) to provide **7Pd** in 55% yield (7.5 mg): R_f (silica−CH_2Cl_2/2% MeOH) = 0.38; ^1H NMR (400 MHz, CD_2Cl_2): δ 8.28 (d, ^3J = 7.7 Hz, 1H), 8.19 (d, ^3J = 7.6, ^4J = 1.1 Hz, 1H), 8.09 (d, ^3J = 4.8 Hz, 1H), 7.73−7.58 (m, 9H) ppm; ^{13}C NMR (100 MHz, CD_2Cl_2): δ 149.9, 144.7, 143.8, 140.7, 139.5, 137.0, 133.6, 133.0, 131.9, 131.4, 129.8, 129.7, 128.3, 128.2, 127.0, 126.9, 126.0, 125.5, 124.5, 109.2 ppm; UV−vis (CH_2Cl_2) λ_{max} (log ε) 323 (4.43), 401 (4.64), 472 (4.48), 668 (4.00), 710 (4.22) nm; IR (neat, diamond ATR): see Figure S48, SI; MS (ESI$^+$, 100% CH_3CN, TOF) m/z cald for $C_{44}H_{25}N_6Pd$ ([M·H]$^+$), 743.1191 found 743.1184.

Bisquinoline-Annulated Porphyrin Quinoline *N*-Oxide $15H_2$. Prepared in 96% isolated yields (20.8 mg) from monofused oxime $\mathbf{14H_2}$ (22.3 mg, 3.31×10^{-4} mmol) dissolved in CH_2Cl_2 (10 mL) and DDQ (16.9 mg, 7.44×10^{-5} mol, ∼2.3 equiv) as described for *N*-oxide **12**: R_f (silica−CH_2Cl_2/10% MeOH) = 0.78; ^1H NMR (400 MHz, $CDCl_3$): δ 9.20 (d, ^3J = 8.0 Hz, 1H), 8.98−8.93 (m, 2H), 8.89 (d, ^3J = 8.0 Hz, 1H), 8.77 (br s, 2H), 8.15 (br s, 1H), 8.10 (d, ^3J = 4.0 Hz, 1H), 7.95−7.82 (m, 10H), 7.75−7.65 (m, 6H), 1.79 (br s, 2H, exchangeable with D_2O) ppm; ^{13}C NMR (100 MHz, $CDCl_3$): δ 145.1, 140.3, 139.6, 133.6, 133.5, 132.2, 131.2, 130.7, 129.6, 128.8, 128.7, 128.5, 127.9, 127.5, 127.4, 126.9, 126.5, 126.0, 125.5, 125.2, 121.2, 102.6 ppm; UV−vis (CH_2Cl_2) λ_{max} (log ε) 412 (4.80), 439 (sh), 485 (sh), 521 (4.12), 568 (3.66), 638 (3.77), 703 (4.14), 779 (4.44) nm; IR (neat, diamond ATR): see Figure S51, SI; MS (ESI$^+$, cone voltage = 30 V, 100% CH_3CN) m/z calcd for $C_{44}H_{27}N_6O$ ([M·H]$^+$) 655.2241, found 655.2221.

■ ASSOCIATED CONTENT

Supporting Information

^1H and ^{13}C NMR and IR spectra of all compounds obtained and experimental details for the crystal structure determinations of **10Ni**, **12Ni**, **7Pd**, and $\mathbf{15H_2}$, including X-ray data (CIF). This material is available free of charge via the Internet at http://pubs.acs.org.

■ AUTHOR INFORMATION

Corresponding Author

*Tel: (+1) 860 486-2743. Fax: (+1) 860 486-2981. E-mail: c.bruckner@uconn.edu.

Notes

The authors declare no competing financial interest.

■ ACKNOWLEDGMENTS

This work was supported by the US National Science Foundation (CHE-0517782 and CHE-1058846). The ApexII X-ray diffractometer was funded by NSF Grant 0087210, Ohio Board of Regents Grant CAP-491, and Youngstown State University. The Prospector X-ray diffractometer was funded by NSF Grant 1337296. We thank Mathias Senge, Trinity College Dublin, for technical advice on the skeletal deviation plots.

■ REFERENCES

(1) (a) Bonnett, R. *Chemical Aspects of Photodynamic Therapy*; Gordon & Breach: Langhorne, PA, 2000. (b) Sternberg, E. D.; Dolphin, D.; Brückner, C. *Tetrahedron* **1998**, *54*, 4151−4202. (c) Ethirajan, M.; Chen, Y.; Joshi, P.; Pandey, R. K. *Chem. Soc. Rev.* **2011**, *40*, 340−362.

(2) Wainwright, M. *Photodiagn. Photodyn. Ther.* **2009**, *6*, 167−169.

(3) Donnelly, R. F.; McCarron, P. A.; Tunney, M. M. *Microbiol. Res.* **2008**, *163*, 1−12.

(4) Weissleder, R.; Pittet, M. J. *Nature* **2008**, *452*, 580−589.

(5) Wilson, P. C. *Photosensitizing Compouds: Their Chemistry, Biology and Clinical Use*; Wiley Interscience: Chichester, 1989.

(6) Cerussi, A. E.; Berger, A. J.; Bevilacqua, F.; Shah, N.; Jakubowski, D.; Butler, J.; Holcombe, R. F.; Tromberg, B. J. *Acad. Radiol.* **2001**, *8*, 211−218.

(7) (a) Li, L.-L.; Diau, E. W.-G. *Chem. Soc. Rev.* **2013**, *42*, 291−304. (b) Gust, D.; Moore, T. A.; Moore, A. L. *Pure Appl. Chem.* **1998**, *70*, 2189−2200. (c) Ball, P. *New Sci.* **1999**, *161*, 38−41. (d) Banala, S.; Rühl, T.; Sintic, P.; Wurst, K.; Kräutler, B. *Angew. Chem., Int. Ed.* **2009**, *48*, 599−603. (e) Alexy, E. J.; Yuen, J. M.; Chandrashaker, V.; Diers, J. R.; Kirmaier, C.; Bocian, D. F.; Holten, D.; Lindsey, J. S. *Chem. Commun.* **2014**, *50*, 14512−14515.

(8) (a) Kim, C.; Favazza, C.; Wang, L. V. *Chem. Rev.* **2010**, *110*, 2756−2782. (b) Wang, L. V. *Nat. Photonics* **2009**, *3*, 503−509.

(9) Abuteen, A.; Zanganeh, S.; Akhigbe, J.; Samankumara, L. P.; Aguirre, A.; Biswal, N.; Braune, M.; Vollertsen, A.; Röder, B.; Brückner, C.; Zhu, Q. *Phys. Chem. Chem. Phys.* **2013**, *15*, 18502−18509.

(10) (a) Sessler, J. L.; Gebauer, A.; Weghorn, S. J. In *The Porphyrin Handbook*; Kadish, K. M., Smith, K. M., Guilard, R., Eds.; Academic Press: San Diego, 2000; Vol. 2, pp 55−124. (b) Sessler, J. L.; Davis, J. M. *Acc. Chem. Res.* **2001**, *34*, 989−997. (c) Pareek, Y.; Ravikanth, M.; Chandrashekar, T. K. *Acc. Chem. Res.* **2012**, *45*, 1801−1816.

(11) (a) Crossley, M. J.; King, L. G.; Newsom, I. A.; Sheehan, C. S. *J. Chem. Soc., Perkin Trans. 1* **1996**, 2675−2684. (b) Kozyrev, A. N.; Suresh, V.; Das, S.; Senge, M. O.; Shibata, M.; Dougherty, T. J.; Pandey, R. K. *Tetrahedron* **2000**, *56*, 3353−3364. (c) Lash, T. D.; Werner, T. M.; Thompson, M. L.; Manley, J. M. *J. Org. Chem.* **2001**, *66*, 3152−3159. (d) Gill, H. S.; Harmjanz, M.; Santamarìa, J.; Finger, I.; Scott, M. J. *Angew. Chem., Int. Ed.* **2004**, 485−490. (e) McCarthy, J. R.; Hyland, M. A.; Brückner, C. *Org. Biomol. Chem.* **2004**, *2*, 1484−1491. (f) Nakamura, Y.; Aratani, N.; Shinokubo, H.; Takagi, A.; Kawai, T.; Matsumoto, T.; Yoon, Z. S.; Kim, D. Y.; Ahn, T. K.; Kim, D.; Muranaka, A.; Kobayashi, N.; Osuka, A. *J. Am. Chem. Soc.* **2006**, *128*, 4119−4127. (g) Diev, V. V.; Hanson, K.; Zimmerman, J. D.; Forrest, S. R.; Thompson, M. E. *Angew. Chem., Int. Ed.* **2010**, *49*, 5523−5526. (h) Jiao, C.; Huang, K.-W.; Guan, Z.; Xu, Q.-H.; Wu, J. *Org. Lett.* **2010**, *12*, 4046−4049. (i) Dudkin, S. V.; Makarova, E. A.; Fukuda, T.; Kobayashi, N.; Lukyanets, E. A. *Tetrahedron Lett.* **2011**, *52*, 2994−2996. (j) Krayer, M.; Yang, E.-K.; Diers, J. R.; Bocian, D. F.; Holten, D.; Lindsey, J. S. *New J. Chem.* **2011**, *35*, 587−601. (k) Brückner, C.; Götz, D. C. G.; Fox, S. P.; Ryppa, C.; McCarthy, J. R.; Bruhn, T.; Akhigbe, J.; Banerjee, S.; Daddario, P.; Daniell, H. W.; Zeller, M.; Boyle, R. W.; Bringmann, G. *J. Am. Chem. Soc.* **2011**, *133*, 8740−8752. (l) Samankumara, L. P.; Wells, S.; Zeller, M.; Acuña, A. M.; Röder, B.; Brückner, C. *Angew. Chem., Int. Ed.* **2012**, *51*, 5757−5760. (m) Ishizuka, T.; Saegusa, Y.; Shiota, Y.; Ohtake, K.; Yoshizawa, K.; Kojima, T. *Chem. Commun.* **2013**, *49*, 5939−5941.

(12) Fox, S.; Boyle, R. W. *Tetrahedron* **2006**, *62*, 10039−10054.

(13) (a) Barloy, L.; Dolphin, D.; Dupre, D.; Wijesekera, T. P. *J. Org. Chem.* **1994**, *59*, 7976−7985. (b) Callot, H. J.; Schaeffer, E.; Cromer, R.; Metz, F. *Tetrahedron* **1990**, *46*, 5253−5262. (c) Richeter, S.; Jeandon, C.; Ruppert, R.; Callot, H. J. *Tetrahedron Lett.* **2001**, *42*, 2103−2106.

(14) (a) Davis, N. K. S.; Pawlicki, M.; Anderson, H. L. *Org. Lett.* **2008**, *10*, 3945−3947. (b) Davis, N. K. S.; Thompson, A. L.; Anderson, H. L. *Org. Lett.* **2010**, *12*, 2124−2127. (c) Davis, N. K. S.; Thompson, A. L.; Anderson, H. L. *J. Am. Chem. Soc.* **2011**, *133*, 30−31.

(15) (a) Ishkov, Y. V.; Zhilina, Z. I. *Zh. Org. Khim.* **1995**, *31*, 136−139. (b) Fouchet, J.; Jeandon, C.; Ruppert, R.; Callot, H. J. *Org. Lett.* **2005**, *7*, 5257−5260. (c) Hyland, M. A.; Morton, M. D.; Brückner, C. *J. Org. Chem.* **2012**, *77*, 3038−3048.

(16) (a) Callot, H. J.; Ruppert, R.; Jeandon, C.; Richeter, S. *J. Porphyrins Phthalocyanines* **2004**, *8*, 111−119. (b) Jimenez, A. J.; Jeandon, C.; Gisselbrecht, J.-P.; Ruppert, R. *Eur. J. Org. Chem.* **2009**, 5725−5730. (c) Richeter, S.; Jeandon, C.; Gisselbrecht, J.-P.; Graff, R.; Ruppert, R.; Callot, H. J. *Inorg. Chem.* **2004**, *43*, 251−263. (d) Richeter, S.; Jeandon, C.; Gisselbrecht, J.-P.; Ruppert, R.; Callot, H. J. *Inorg. Chem.* **2007**, *46*, 10241−10251. (e) Richeter, S.; Jeandon, C.; Kyritsakas, N.; Ruppert, R.; Callot, H. J. *J. Org. Chem.* **2003**, *68*, 9200−9208. (f) Richeter, S.; Christophe, J.; Jean-Paul, G.; Romain, R. In *Handbook of Porphyrin Science*; World Scientific Publishing Company: Hackensack, NJ, 2010; Vol. Vol. 3, pp 429−483.

(17) Jeandon, C.; Ruppert, R. *Eur. J. Org. Chem.* **2011**, 4098−4102.

(18) Akhigbe, J.; Zeller, M.; Brückner, C. *Org. Lett.* **2011**, *13*, 1322−1325.

(19) Daniell, H. W.; Williams, S. C.; Jenkins, H. A.; Brückner, C. *Tetrahedron Lett.* **2003**, *44*, 4045−4049.

(20) (a) Crossley, M. J.; King, L. G. *J. Chem. Soc., Chem. Commun.* **1984**, 920−922. (b) Crossley, M. J.; Burn, P. L.; Langford, S. J.; Pyke, S. M.; Stark, A. G. *J. Chem. Soc., Chem. Commun.* **1991**, 1567−1568. (c) Starnes, S. D.; Arungundram, S.; Saunders, C. H. *Tetrahedron Lett.* **2002**, *43*, 7785−7788. (d) Starnes, S. D.; Rudkevich, D. M.; Rebek, J., Jr. *Org. Lett.* **2000**, *2*, 1995−1998.

(21) Akhigbe, J.; Brückner, C. *Eur. J. Org. Chem.* **2013**, 3876−3884.

(22) Brückner, C.; McCarthy, J. R.; Daniell, H. W.; Pendon, Z. D.; Ilagan, R. P.; Francis, T. M.; Ren, L.; Birge, R. R.; Frank, H. A. *Chem. Phys.* **2003**, *294*, 285−303.

(23) (a) Buchler, J. W. In *Porphyrins*; Dolphin, D., Ed.; Academic Press: New York, 1978; Vol. 1, pp 389−483. (b) Dean, M. L.; Schmink, J. R.; Leadbeater, N. E.; Brückner, C. *Dalton Trans.* **2008**, 1341−1345.

(24) (a) Xiao, H.-L.; Zeng, C.-C.; Tian, H.-Y.; Hu, L.-M.; Little, R. D. *J. Electroanal. Chem.* **2014**, *727*, 120−124. (b) Li, W.; Jia, P.; Han, B.; Li, D.; Yu, W. *Tetrahedron* **2013**, *69*, 3274−3280. (c) Dolka, C.; Van Hecke, K.; Van Meervelt, L.; Tsoungas, P. G.; Van der Eycken, E. V.; Varvounis, G. *Org. Lett.* **2009**, *11*, 2964−2967. (d) Desai, V. G.; Naik, S. R.; Dhumaskar, K. L. *Synth. Commun.* **2014**, *44*, 1453−1460.

(25) Yashunsky, D. V.; Morozova, Y. V.; Ponomarev, G. V. *Chem. Heterocycl. Compd.* **2001**, *37*, 380−381.

(26) Wang, H.; Zhu, M.; Ye, S.; Wu, J. *RSC Adv.* **2013**, *3*, 13626−13629.

(27) (a) Andrews, L. E.; Bonnett, R.; Ridge, R. J.; Appelman, E. H. *J. Chem. Soc., Perkin Trans. 1* **1983**, 103−107. (b) Groves, J. T.; Watanabe, Y. *J. Am. Chem. Soc.* **1986**, *108*, 7836−7837. (c) Banerjee, S.; Zeller, M.; Brückner, C. *J. Org. Chem.* **2009**, *74*, 4283−4288.

(28) Pietra, A. A. S. *Heterocyclic N-Oxides*; CRC Press: Boca Raton, 1991.

(29) (a) Jaquinod, L.; Gros, C.; Olmstead, M. M.; Antolovich, M.; Smith, K. M. *Chem. Commun.* **1996**, 1475−1476. (b) Gros, C. P.; Jaquinod, L.; Khoury, R. G.; Olmstead, M. M.; Smith, K. M. *J. Porphyrins Phthalocyanines* **1997**, *1*, 201−212.

(30) (a) Olofson, R. A.; Michelman, J. S. *J. Org. Chem.* **1965**, *30*, 1854−1859. (b) Behr, L. C.; Brent, J. T. *Org. Synth.* **1954**, *34*, 40−41.

(31) (a) Barkigia, K. M.; Renner, M. W.; Furenlid, L. R.; Medforth, C. J.; Smith, K. M.; Fajer, J. *J. Am. Chem. Soc.* **1993**, *115*, 3627−3635. (b) Sparks, L. D.; Medforth, C. J.; Park, M. S.; Chamberlain, J. R.; Ondrias, M. R.; Senge, M. O.; Smith, K. M.; Shelnutt, J. A. *J. Am. Chem. Soc.* **1993**, *115*, 581−592. (c) Brückner, C.; Hyland, M. A.; Sternberg, E. D.; MacAlpine, J.; Rettig, S. J.; Patrick, B. O.; Dolphin, D. *Inorg. Chim. Acta* **2005**, *358*, 2943−2953.
(32) Richeter, S.; Jeandon, C.; Ruppert, R.; Callot, H. J. *Chem. Commun.* **2001**, 91−92.
(33) Senge, M. O. In *Porphyrin Handbook*; Kadish, K. M., Smith, K. M., Guilard, R., Eds.; Academic Press: San Diego, 2000; Vol. *10*, pp 1−218.
(34) (a) Ryeng, H.; Ghosh, A. *J. Am. Chem. Soc.* **2002**, *124*, 8099−8103. (b) Lebedev, A. Y.; Filatov, M. A.; Cheprakov, A. V.; Vinogradov, S. A. *J. Phys. Chem. A* **2008**, *112*, 7723−7733. (c) Röder, B.; Büchner, M.; Rückmann, I.; Senge, M. O. *Photochem. Photobiol. Sci.* **2010**, *9*, 1152−1158.